ACS NANO

www.acsnano.org

ARTICLE

The Effects of Extensive Glomerular Filtration of Thin Graphene Oxide Sheets on Kidney Physiology

Dhifaf A. Jasim,[†,‡] Stephanie Murphy,[§] Leon Newman,[†,‡] Aleksandr Mironov,[∥] Eric Prestat,[‡,⊥] James McCaffrey,[§,#] Cécilia Ménard-Moyon,[▽] Artur Filipe Rodrigues,[†,‡] Alberto Bianco,[▽] Sarah Haigh,[‡,⊥] Rachel Lennon,[*,§,#] and Kostas Kostarelos[*,†,‡]

[†]Nanomedicine Laboratory, Faculty of Biology, Medicine and Health, [‡]National Graphene Institute, [§]Wellcome Trust Centre for Cell-Matrix Research, [∥]TEM Facility, and [⊥]School of Materials, University of Manchester, Manchester M13 9PL, United Kingdom

[#]Department of Pediatric Nephrology, Royal Manchester Children's Hospital, Central Manchester University Hospitals NHS Foundation Trust (CMFT), Manchester Academic Health Science Centre, Manchester M13 9NT, United Kingdom

[▽]University of Strasbourg, CNRS, Immunopathology and Therapeutic Chemistry, UPR 3572, 67000 Strasbourg, France

S *Supporting Information*

ABSTRACT: **Understanding how two-dimensional (2D) nanomaterials interact with the biological milieu is fundamental for their development toward biomedical applications. When thin, individualized graphene oxide (GO) sheets were administered intravenously in mice, extensive urinary excretion was observed, indicating rapid transit across the glomerular filtration barrier (GFB). A detailed analysis of kidney function, histopathology, and ultrastructure was performed, along with the *in vitro* responses of two highly specialized GFB cells (glomerular endothelial cells and podocytes) following exposure to GO. We investigated whether these cells preserved their unique barrier function at doses 100 times greater than the dose expected to reach the GFB *in vivo*. Both serum and urine analyses revealed that there was no impairment of kidney function up to 1 month after injection of GO at escalating doses. Histological examination suggested no damage to the glomerular and tubular regions of the kidneys. Ultrastructural analysis by transmission electron microscopy showed absence of damage, with no change in the size of podocyte slits, endothelial cell fenestra, or the glomerular basement membrane width. The endothelial and podocyte cell cultures regained their full barrier function after >48 h of GO exposure, and cellular uptake was significant in both cell types after 24 h. This study provided a previously unreported understanding of the interaction between thin GO sheets with different components of the GFB *in vitro* and *in vivo* to highlight that the glomerular excretion of significant amounts of GO did not induce any signs of acute nephrotoxicity or glomerular barrier dysfunction.**

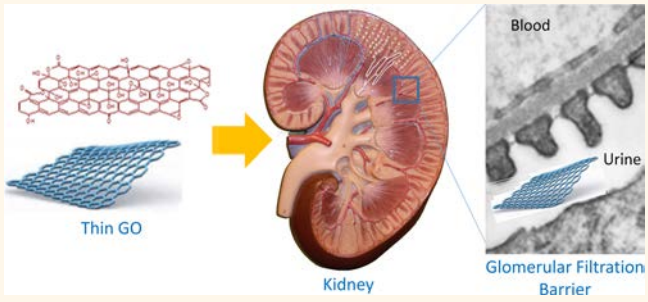

KEYWORDS: *2D crystals, carbon nanomaterial, urinary excretion, nanotoxicology*

Graphene has a unique two-dimensional (2D) carbon geometry that results in a variety of exceptional physicochemical properties.[1,2] These properties have attracted great interest in different scientific disciplines and for wide-ranging applications, from physics to materials science and, more recently, biomedicine.[3−5] Large surface area,[6−8] high mechanical strength,[9−12] and flexibility[3,13] are some of the unique characteristics by which the material interacts with soft biological matter. Graphene oxide (GO), the oxidized analogue of graphene, also contains an abundance of oxygenated functions on both sides of the planar structure that makes the material more hydrophilic and highly charged electrostatically compared to graphene. The use of GO has expanded the applications of graphene-based materials in biomedicine due to its improved dispersibility in aqueous environments and the capacity for further introduction of functional moieties on the surface of these 2D sheets.[14]

The most popular administration route used in the preclinical development of GO for biomedical applications has been the intravenous (i.v.).[15] Extensive urinary excretion of GO has also been reported in several studies after i.v. injection

Received: May 20, 2016
Accepted: November 23, 2016
Published: November 28, 2016

DOI: 10.1021/acsnano.6b03358
ACS Nano 2016, 10, 10753−10767

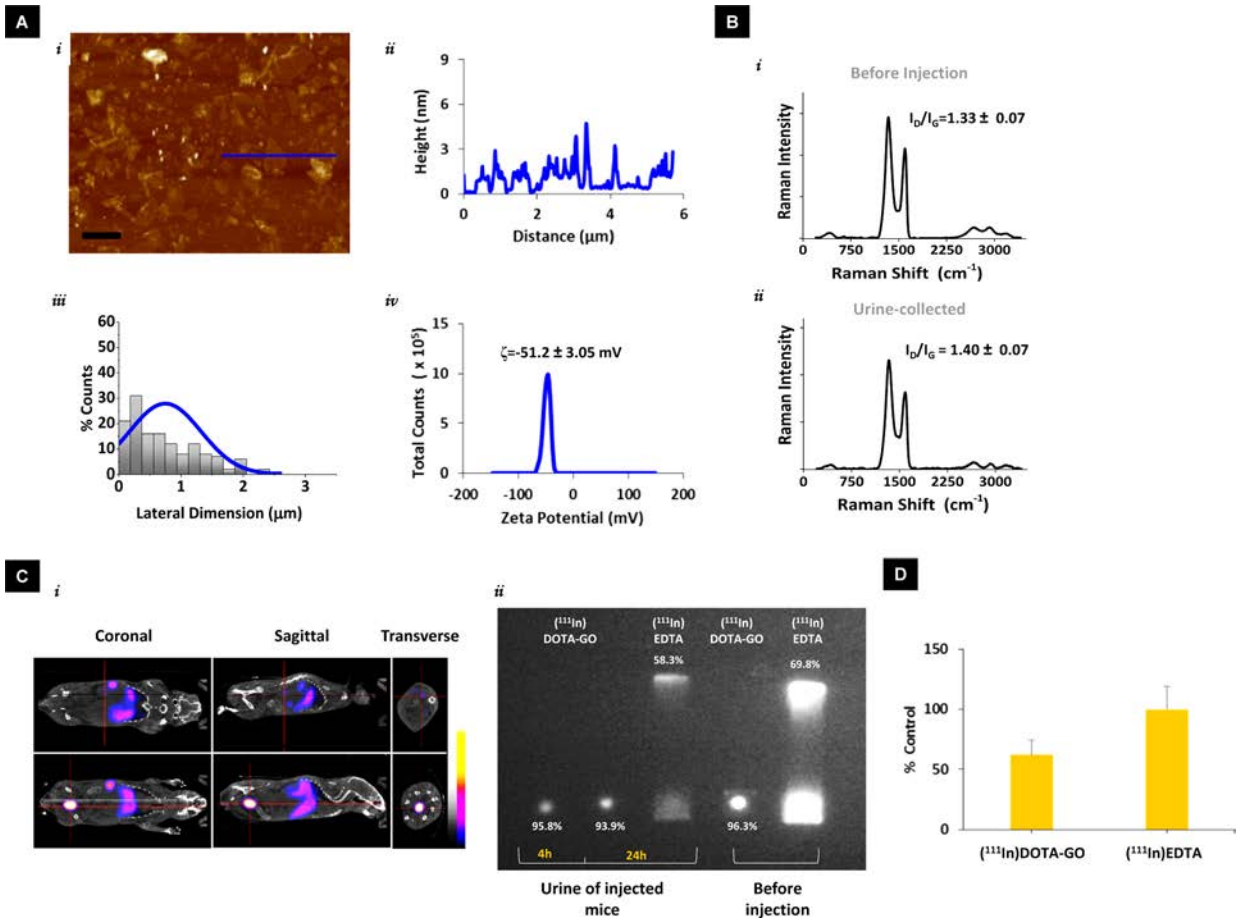

Figure 1. Graphene oxide before injection and after detection in urine of injected mice: (A) characterization of GO by (*i*) AFM imaging; (*ii*) AFM height section of the blue line in *i*; (*iii*) lateral size distribution obtained by counting more than 100 GO sheets from the AFM image in *i*; and (*iv*) surface charge of GO represented by zeta potential values (values are mean ± SD; $n = 3$). (B) GO in solution and GO from the urine of mice 24 h postinjection by Raman spectroscopy of the GO before injection (*i*) of the GO excreted in urine (*ii*). All Raman spectra were an average of five spectra ($n = 5$). (C) (*i*) SPECT/CT images of a C57BL/6 mouse injected with (^{111}In)DOTA-GO, showing coronal, sagittal, and transverse views of the kidney (top) and bladder (bottom); images were captured at 0−1 h after injection. (*ii*) *In vivo* stability of (^{111}In)DOTA-GO, as detected by TLC; first three columns indicate the excretion of intact (^{111}In)DOTA-GO and (^{111}In)EDTA) in the urine of injected mice, compared to the doses before injection (last two columns). (D) Excreted dose of (^{111}In)DOTA-GO in the urine of injected mice represented as percent of radioactivity collected from control (^{111}In)EDTA; urine was extracted by direct bladder intervention. AFM images scale bars are 2 μm.

of functionalized GO sheets in mice.[8,16−20] The glomerulus is the main filtration organelle in the kidney,[21] and GO sheets are thought to be excreted by crossing the glomerular filtration barrier (GFB). However, no direct experimental evidence has been reported to validate such excretion mechanism today.

The GFB contains (among other acellular components) two highly specialized cellular components: the fenestrated glomerular endothelial cells (GEnC) and the glomerular epithelial cells known as the podocytes.[22,23] The GEnC make up the initial cellular barrier encountered by blood-circulating nanomaterials as they reach the glomerular capillaries and they have fenestra estimated at ∼60 nm in width.[22−24] The podocytes are highly specialized and differentiated cells with large cell bodies and finger-like protrusions (termed the foot processes) that bulge into the urinary side of the GFB.[25] The foot processes are separated by slits that have been reported to be 25−60 nm wide, and these are formed by a specialized cell−cell junction known as the slit diaphragm. The podocytes support the glomerular basement membrane (BM) and are critical for the selective permeability of the glomerular filter. The glomerular BM is composed of a fibrous network containing predominantly collagen IV-alpha 3,4,5 and laminin-521 among other proteins that are secreted by podocytes and GEnC.[23,25,26] Although the glomerular endothelial fenestra and the podocyte slit sizes are reported to be between 60 and 40 nm,[23,25,27] the prevention of the relatively small albumin (ALB) molecules (diameter only 3.6 nm, molecular weight 66.5 kDa) to pass through the kidney suggests that the GFB permselectivity is a much more sophisticated process.

In previous reports, we have shown by whole-body single-photon and positron emission computed tomography (SPECT/CT)[19] and (PET/CT)[20] imaging as well as cut-and-count radioactivity measurements[19] the detailed pharmacokinetics and tissue distribution of thin GO sheets upon i.v. administration. The GO entered systemic blood circulation, and a significant fraction (>50%) of the injected dose was excreted in the urine at early time points. Similar findings have also been reported by others.[8,16−18] However, very little has been described on both the interaction of these 2D materials with the GFB and whether such interactions can have an adverse impact on kidney tissue structure and function. In this study we interrogated the function as well as the histological

DOI: 10.1021/acsnano.6b03358
ACS Nano 2016, 10, 10753−10767

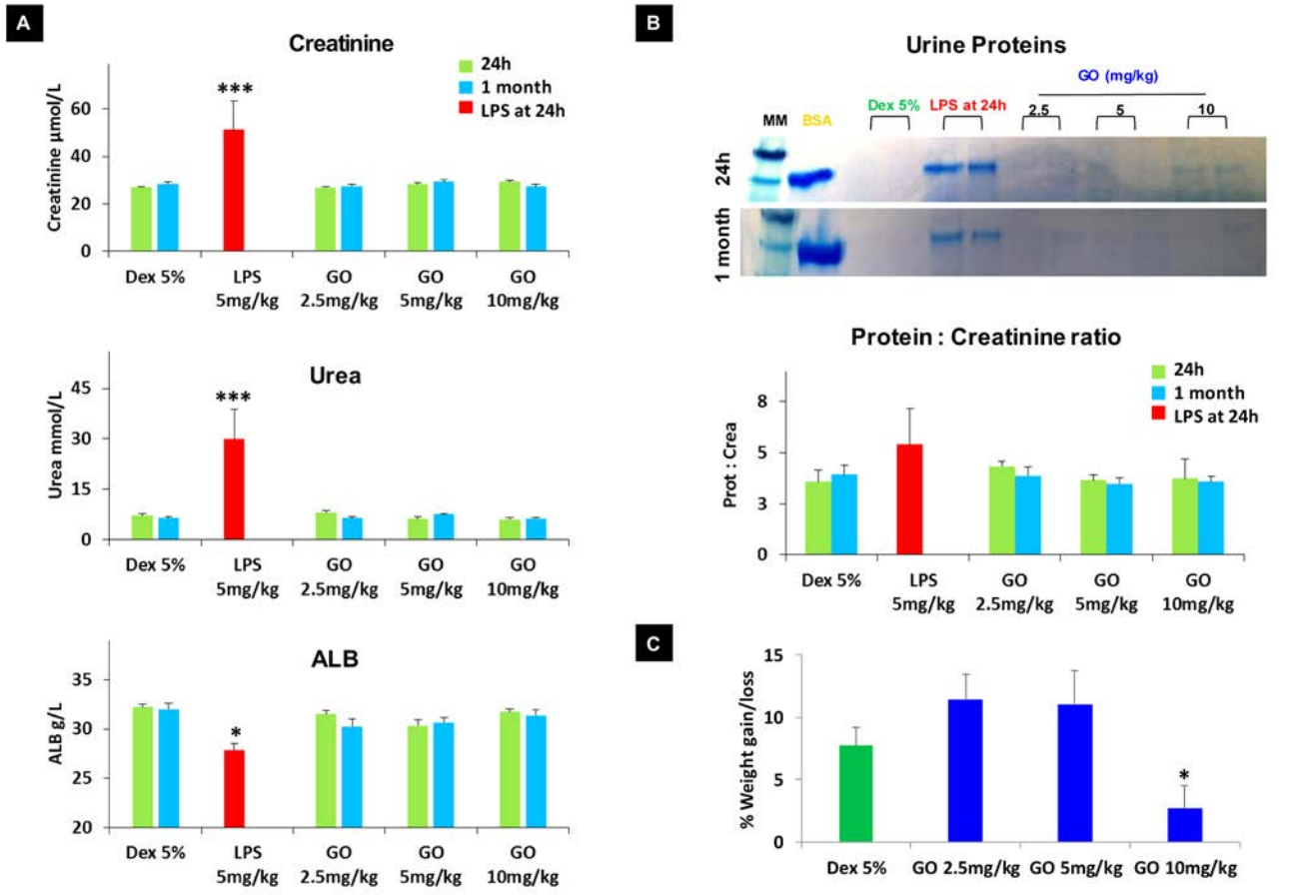

Figure 2. Kidney function analysis and mice weight change. Mice (n = 4 mice for each group) injected with three different doses of GO (2.5, 5, and 10 mg/kg) compared to control-injected mice (LPS 5 mg/kg and Dex 5%) at 1 day and 1 month after injection: (A) Serum analysis, from top to bottom, shows serum levels of creatinine, urea, and albumin. (B) Urine analysis showing SDS gels (top) of urine collected 24 h and 1 month after injection; bottom graph shows protein:creatinine ratio. (C) Animal body weight (represented as percent of weight gain) in mice injected with three different doses of GO (2.5, 5, and 10 mg/kg) and control-injected mice (Dex 5%) 1 month after injection. All data are represented as mean ± standard error (SE). Statistical significance was tested using one-way ANOVA with Tukey's *posthoc* test ($p < 0.005$ * and $p < 0.05$ *). MM in B stands for molecular marker or reference protein ladder.**

and ultrastructural morphology of the kidney tissue in C57BL/6 mice following administration of increasing amounts of GO. We further investigated the effects of GO sheets on cell culture models of GEnC and podocytes to obtain a more thorough understanding of the potential impact on the mechanism of interaction between GO sheets and these cells as well as the impact on the barrier function at excessive GO dose exposure regimes.

RESULTS

Preparation and Characterization of GO. Graphene oxide was prepared by a modified Hummers' method using chemical oxidation in strong acidic conditions, followed by thorough characterization of the resulting thin GO material used in the present work.[28] GO-DOTA (DOTA: 1,4,7,10-tetraazacyclododecane-1,4,7,10-tetraacetic acid) was prepared from GO by a two-step derivatization process.[19] That previous report showed by XPS analysis that the C/O ratio increased only slightly after derivatization with DOTA from 2.3 (for GO) to 2.4, which indicated that the presence of DOTA did not dramatically affect the surface properties of the starting material. Figure 1A*i* shows atomic force microscopy (AFM) data of several GO sheets and the height profile across the blue line (Figure 1A*ii*). The thickness of the prepared GO was 1−2 nm, corresponding to 1−3 single sheets. The size distribution of GO sheets was quite wide, as reported previously,[28] however the vast majority (>70%) of the sheets had a lateral dimension below 1 μm (Figure 1A*iii*). The mean surface charge of the GO sheets was highly negative with a zeta potential of −51.2 ± 3.1 mV (Figure 1A*iv*). The Raman spectrum (Figure 1B*i*) shows the characteristic G and D bands of the GO. The G band at 1595 cm^{-1} is due to bond stretching of sp^2 hybridized carbon atoms, and the prominent disorder D band was at 1330 cm^{-1}. The 2D band near 2700 cm^{-1} was almost absent, and the D to G band intensity ratio (I_D/I_G), corresponding to the metric of disorder is shown in the inset. The G band, indicative of sp^2 hybridized carbon atoms, was present at around 1590 cm^{-1}.[9,29]

Urinary Excretion of GO. Intravenous administration of the as-prepared GO sheets through the tail vein of mice resulted in the presence of GO sheets in their urine 24 h postinjection.[19] Raman spectroscopy confirmed the presence of GO in the urine, and the D to G band intensity ratio (I_D/I_G) is shown in the legend (Figure 1B*ii*). As described in our previous work,[19] aqueous GO dispersions were functionalized with the chelating agent DOTA and efficiently and stably radiolabeled with (^{111}In) for imaging. The excretion of (^{111}In)DOTA-GO was again evidenced here by SPECT/CT in Figure 1C*i*,

DOI: 10.1021/acsnano.6b03358
ACS Nano 2016, 10, 10753−10767

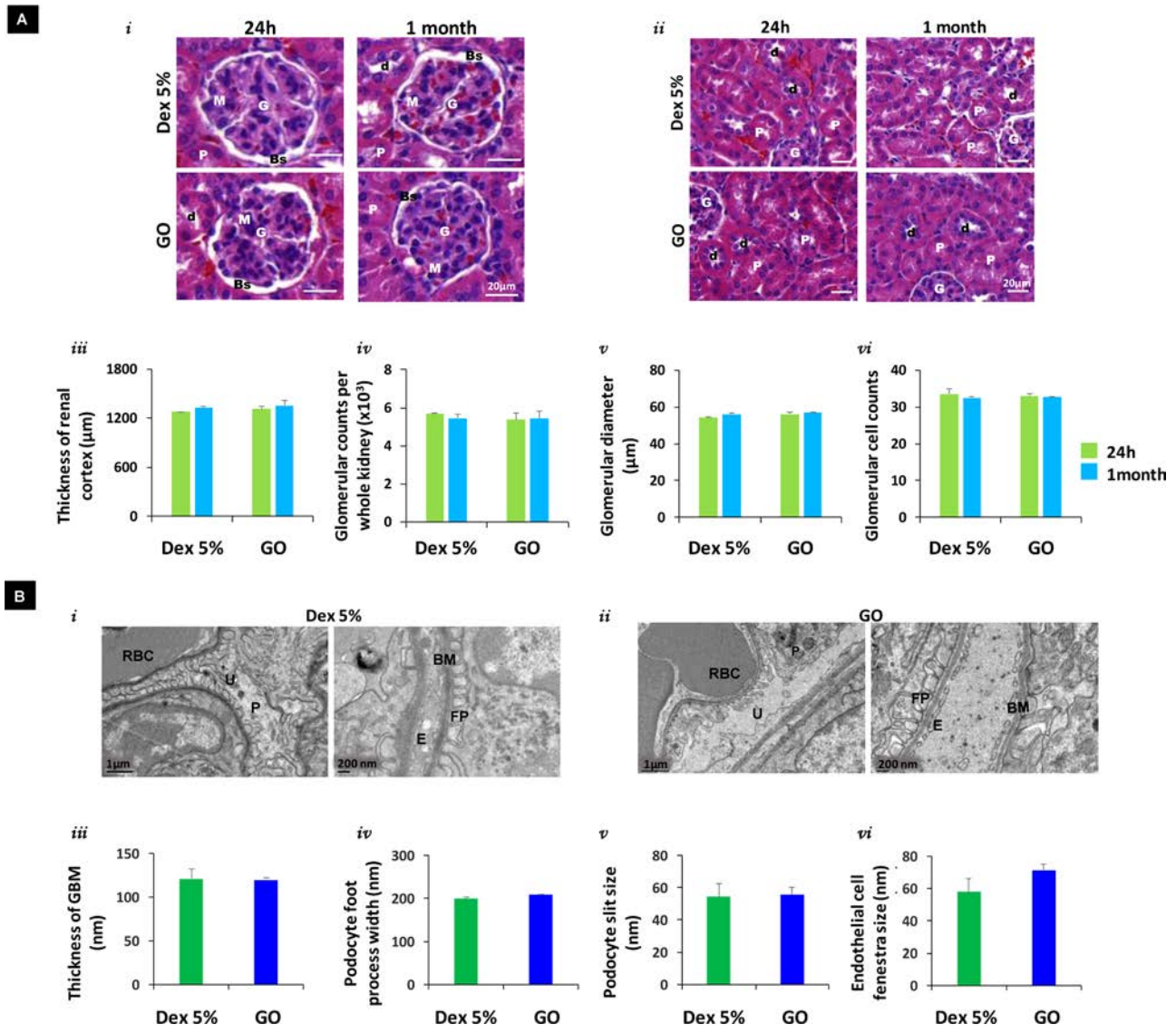

Figure 3. Kidney histology and ultrastructure: (A) Histological examinations of kidneys (*i*–*iv*) renal pathology estimation using different measurements, such as a scoring system, thickness of the renal cortex, number of glomeruli per whole kidney, longitudinal diameter of glomerulus, and number of cells per glomerulus, respectively. Measurements were carried out using at least 50 glomeruli in several kidney sections from two different mice. All values are mean ± SE, and statistical significance was tested using one-way ANOVA with Tukey's *posthoc* test. (*v*) Histology sections showing normal kidney glomerulus and (*vi*) normal renal tubules in GO-injected mice as compared to mice injected with Dex 5% at 24 h and 1 month after the injection. (B) TEM morphometry (*i*–*iv*) represents measurements of GBM thickness, podocyte foot process width, podocyte slit size, and endothelial cell fenestra sizes, respectively. Values are mean of several TEM images captured from two different mice. All values are mean ± SE, and statistical significance was determined by Student's *T* test. (*v*) TEM images comparing a control (Dex 5%)-injected mouse to a GO-injected mouse in (*vi*). G: glomerulus, Bs: Bowman's space, M: mesangium, p: proximal convoluted tubule, d: distal convoluted tubule, RBC: red blood cell, U: urine compartment, P, podocyte, E: endothelial cell, FP: foot processes, BM: glomerular basement membrane.

showing coronal, sagittal, and transverse views of the kidney (top) and bladder (bottom).

To further validate the excretion and radiolabeling stability of the material, urine samples were collected from mice treated with (^{111}In)DOTA-GO at 4 h and 24 h postinjection, and thin-layer chromatography (TLC) spotted in comparison to the material before injection (Figure 1C*ii*). The excreted (^{111}In)-DOTA-GO remained intact and radiolabeled in the urine to confirm the *in vivo* stability of the material. The injected dose excreted in the urine was determined more accurately in a separate experiment by direct bladder puncture (Figure 1D). The excreted dose of (^{111}In)DOTA-GO was 50–60% of the control (^{111}In)EDTA (the latter known to be excreted almost entirely within the first few hours postinjection).[19,20]

The direct visualization of GFB translocation by the GO sheets was attempted next. The same dose of nonradiolabeled GO dispersed in 5% dextrose (2.5 mg/kg) was injected i.v. (tail vein), and the kidney tissues were retrieved 30 min postadministration for scanning transmission electron microscopy (STEM) examination. Figures S1A and B show STEM data of the cross-sectioned glomeruli injected with control dextrose 5% (Dex 5%) and GO. Imaging indicated electron-dense structures (Figure S1B) resembling GO sheets viewed side-on only in the tissue sections of GO-injected mice, that were not present in the tissues from dextrose-injected animals,

DOI: 10.1021/acsnano.6b03358
ACS Nano 2016, 10, 10753–10767

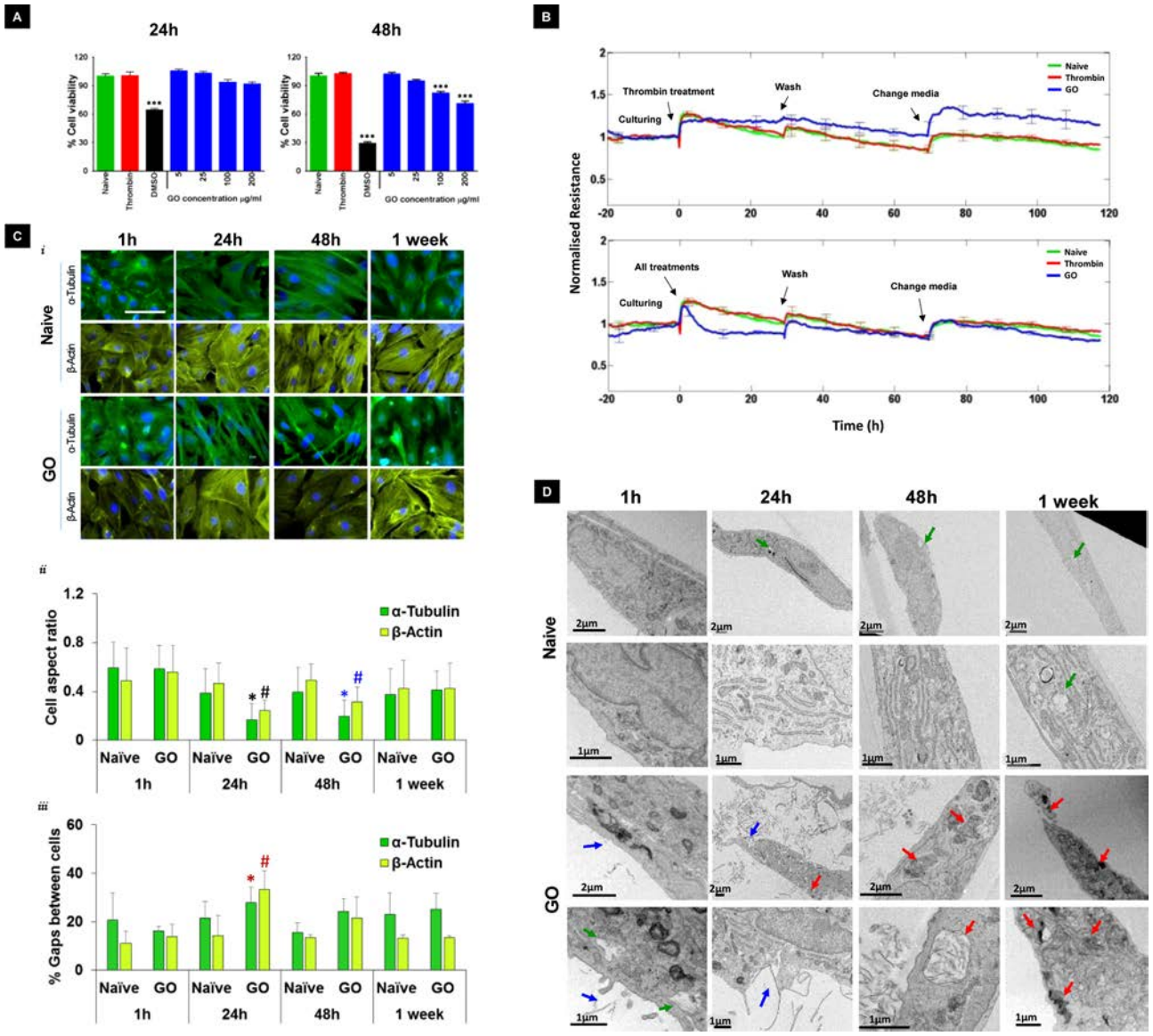

Figure 4. Effect of GO on endothelial cell structure and function: (A) Cytotoxicity of endothelial cells treated with GO (5, 25, 100, and 200 μg/mL) as compared to that of controls (naïve or injected with thrombin or DMSO 10%), as determined by the modified LDH assay, at 24 and 48 h after treatment (left and right, respectively). Statistical significance was determined by using one-way ANOVA with Tukey's *posthoc* test (*: $p < 0.005$ *versus* naïve cells). (B) ECIS evaluation of endothelial cell function of cells pretreated with GO 1 day before culturing them on the ECIS plates (top) and cells treated directly on the ECIS plate (bottom). Cells treated with GO (25 μg/mL) were compared with naïve (untreated cells) and thrombin-treated cells (positive control). (C) Cell morphology detected by (*i*) fluorescence microscopy images after staining cells with α-tubulin (green), β-actin (yellow), and DAPI (blue) at 1 h, 24 h, 48 h and 1 week after treatment with GO (25 μg/mL), as compared to naïve cells. Scale bar is 10 μm. (*ii*) Graph represents the cell aspect ratio, indicative of cell morphology. (*iii*) Graph represents the percentage of gaps detected between cells at the different time points. Graphs were detected by ImageJ analysis using several fields of view for each condition. Statistical significance was determined by using one-way ANOVA with Tukey's *posthoc* test (black *: $p < 0.005$ *versus* naïve cells and GO, at 1 h and 1 week; blue *: $p < 0.005$ *versus* GO at 1 h, $p < 0.01$ *versus* naïve, $p < 0.5$ *versus* GO at 1 week; black #: $p < 0.01$ *versus* naïve, $p < 0.005$ *versus* GO at 1 h; blue #: $p < 0.005$ *versus* GO at 1 h; red * and #: $p < 0.5$ *versus* naïve). (D) TEM images of endothelial cells treated with 25 μg/mL of GO compared to those of naïve cells. Cells were stored for 1 week, washed once with media, which was replaced every 2 days. Green arrows indicate empty vesicles, red arrows indicate vesicles packed with GO, and blue arrows indicate interactions between GO and cell membrane.**

and these structures were thought to represent GO sheets. However, we were not able to decipher unequivocally that these structures were the excreted GO sheets. Further work with more sophisticated techniques is certainly warranted.

Effect of GO on Kidney Function and Structure. To determine the potential impact of the significant GO urinary excretion on renal pathophysiology, groups of C57BL/6 mice were injected i.v. with GO at a dose escalation regime from 2.5 to 10 mg/kg. A range of kidney function analyses are shown in Figure 2, along with the results of blood serum and urine analyses (Figure 2A,B). Overall, no significant differences were noted in the serum levels of creatinine, urea, and ALB in all groups injected with GO at all three doses (2.5, 5, and 10 mg/kg) compared to the control group (5% dextrose alone), both at 1 day and 1 month postinjection. A group of animals injected with lipopolysaccharide (LPS at 5 mg/kg), used here as a

DOI: 10.1021/acsnano.6b03358
ACS Nano 2016, 10, 10753−10767

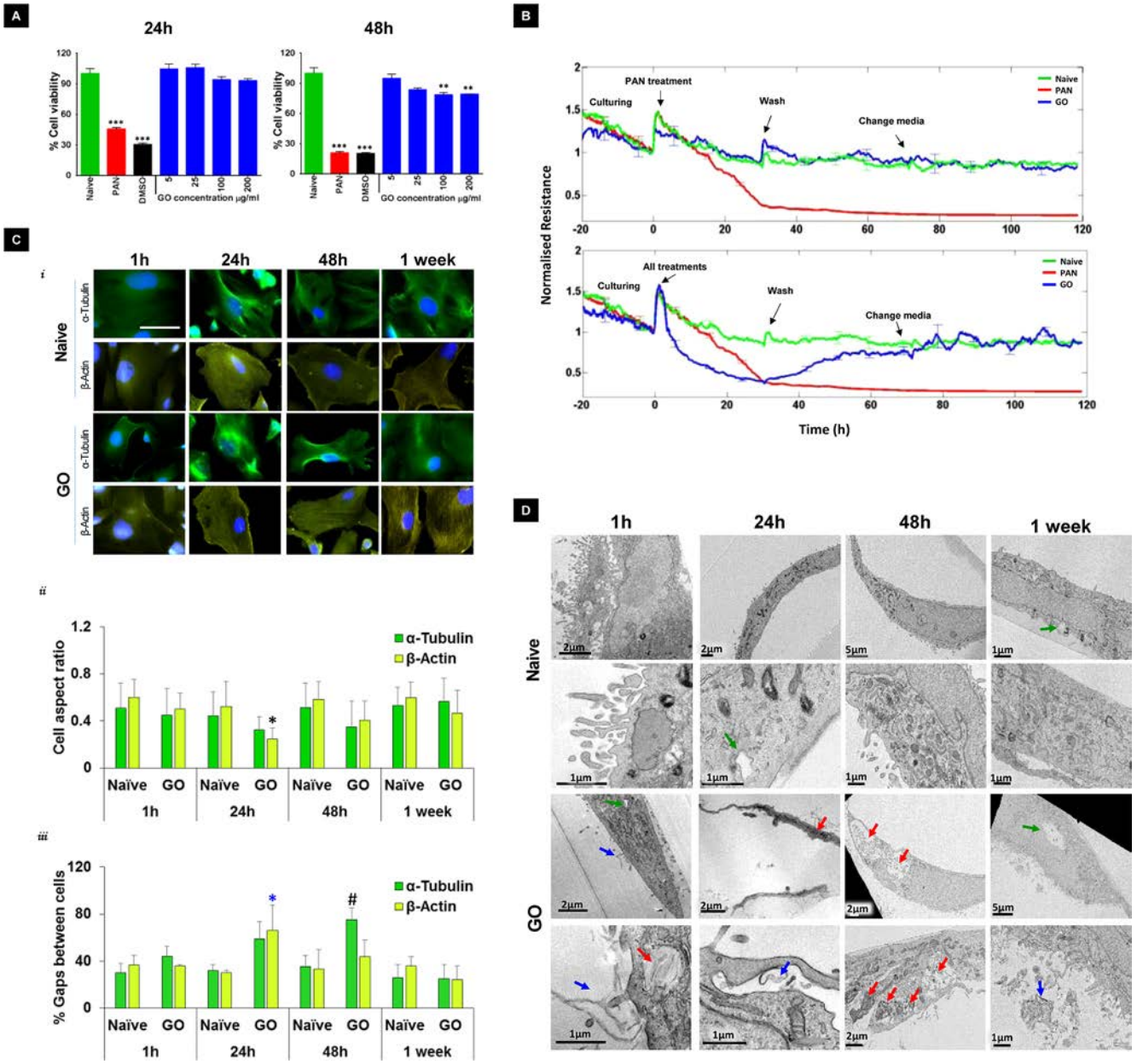

Figure 5. Effect of GO on cell structure and function of podocyte: (A) Cytotoxicity of podocytes treated with GO (5, 25, 100, and 200 μg/mL) compared to that of controls (naïve or treated with PAN and DMSO 10%), as determined by the modified LDH assay 24 and 48 h after treatment (left and right, respectively). Statistical significance was determined by using one-way ANOVA with Tukey's *posthoc* test (: $p < 0.01$ and ***: $p < 0.005$ *versus* naïve cells). (B) ECIS evaluation of cell function of podocytes pretreated with GO 1 day before culturing them on the ECIS plates (top) and cells treated directly on the ECIS plate (bottom). Cells treated with GO (25 μg/mL) were compared to naïve (untreated cells) and PAN-treated cells. (C) Cell morphology detected by (*i*) fluorescence microscopy after staining cells with α-tubulin (green), β-actin (yellow), and DAPI (blue) at 1 h, 24 h, 48 h, and 1 week after treatment with GO (25 μg/mL) and compared with naïve cells. Scale bar is 10 μm. (*ii*) Graph represents the cell aspect ratio which is indicative of cell morphology. (*iii*) Graph represents the percentage of gaps detected between cells at the different time points, detected by ImageJ analysis using several fields of view for each condition. Statistical significance was determined by using one-way ANOVA with Tukey's *posthoc* test (black *: $p < 0.5$ *versus* naïve; blue *: $p < 0.01$ *versus* GO at 1 week, #: $p < 0.01$ *versus* GO at 1 week, and $p < 0.5$ *versus* naïve). (D) TEM images of podocytes treated with 25 μg/mL of GO compared to naïve cells. Cells were stored for 1 week and washed once with media, which was replaced every 2 days. Green arrows indicate empty vesicles, red arrows indicate vesicles packed with GO, and blue arrows indicate interactions between GO and cell membrane.**

nephrotoxic positive control, showed significantly altered serum values demonstrating kidney dysfunction.

Urine proteins (collected by the urine spot collection method) were detected using SDS gels (Figure 2B), and only LPS-injected mice showed significant amount of ALB after 24 h. Only insignificant traces of ALB were detected in the urine of mice injected with the highest GO dose (10 mg/kg). No significance was detected in any other group compared to the dextrose-injected control group. The ratio of serum total protein to serum creatinine level was also measured (Figure 2B bottom), and a slight increase was noted in the LPS-injected group. The differences between the ratios in all groups and the dextrose-control group did not show any statistical significance. Figure 2C displays the percentage increase in the mice body

DOI: 10.1021/acsnano.6b03358
ACS Nano 2016, 10, 10753−10767

weight over a period of 1 month. The weight gain of mice injected with the highest GO dose (10 mg/kg) was significantly less than that in the other two dosing groups (animal weight curves for the different groups are shown in Figure S2), indicative of a toxicity threshold.

In order to avoid possible complications in our analyses, we next looked at the histological impact of GO renal filtration on the kidney tissue using hematoxylin and eosin (H&E) staining after treatment with 7.5 mg/kg, at the high end of the subcytotoxic GO dose regime (Figure 3A). Microscopic analysis of the tissue sections indicated no damage or change of glomerular structure, with intact glomerular (G), mesangial (M), and Bowman's space (Bs). Morphometric analysis was based on various renal pathology benchmarks, including thickness of the renal cortex, number of glomeruli per whole kidney, longitudinal diameter of glomerulus, and number of cells per glomerulus. No significant differences were shown between the various groups and the control-injected group. No signs of inflammatory infiltration, increased cellularity, fibrosis, and/or necrosis were detected in the glomerulus, and intact tubular regions with normal histology were obtained throughout this study.

Ultrastructural analysis of the glomerular endothelium and podocyte foot processes by transmission electron microscopy (TEM) imaging of tissue cross sections was also performed (Figure 3B). The results from the semiquantitative analysis of several TEM images depicted glomerular BM thickness, podocyte foot process width, podocyte slit size, and endothelial cell fenestra sizes. Overall, no statistical differences were detected throughout, with Figure 3B*v*,*vi* indicating normal renal ultrastructure, with no damage to the endothelium and normal podocyte foot processes in the control- and GO-injected mice, respectively.

***In Vitro* Interaction of GO with Kidney Cells.** The two highly specialized cellular components of the GFB separated from each other by the BM are the fenestrated GEnC and the underlying glomerular podocytes.[22,23] We studied the effects of GO sheet exposure on culture models of these two human cell types (Figures 4, 5, and S3−7).

The conditionally immortalized human GEnC cells[30] were treated with GO at different concentrations (5, 25, 100, and 200 μg/mL). Figure 4A demonstrates the percentage of cell viability determined by a modified lactate dehydrogenase (LDH) assay 24 and 48 h after treatment. A significant reduction in cell viability was only detected after 48 h at high concentrations (100, 200 μg/mL). These results were independently confirmed using the Trypan blue cell exclusion assay, with significant cell death occurring only after 48 h at 100 and 200 μg/mL GO concentrations (Figure S3). Next, we examined the effect of GO on the cell barrier function by electric cell−substrate cell impedance sensing (ECIS). Figure 4B (top graph) shows the barrier function of GEnC cells pretreated with 25 μg/mL of GO 24 h before culturing on the ECIS plate, while the bottom graph demonstrates the barrier function of GEnC cells that were directly treated on the ECIS plate. All cells were washed after 24 h, the cell culture media was changed every 2 days, and barrier monitored under ECIS for 1 week. When the cells were pretreated with GO, they retained slightly higher resistance compared to untreated and thrombin (positive control) treated cells. Upon treatment with GO directly on the ECIS plate, the cells exhibited a significant reduction in the resistance, however, they recovered and reached the naïve cell level 48 h after treatment. Thrombin treatment resulted in the expected transient reduction of resistance[31] within 1 h after treatment (Figure S4).

GEnC cell morphology was studied by immunocytochemistry of the cell cytoskeleton with α-tubulin and β-actin (Figures 4C and S5). Figures 4C*i* and S5 demonstrate a change in cell morphology with cellular narrowing and contraction starting at 24 h. This was confirmed by the semiquantitative analysis in Figure 4C*ii*,*iii*, and the cell aspect ratio (a measure of cell morphology) that indicated significant changes at 24 h after treatment, with gradual recovery starting at 48 h and reaching full recovery after 1 week. The distance between cells (Figure 4C*iii*) also increased, confirming cell contraction, and in this data, a similar pattern of recovery was noted after 1 week. TEM imaging of fixed GEnC cells following treatment with GO at different time points compared to untreated cells (naïve) was then carried out (Figures 4D and S6A). GO sheets were seen to interact with the plasma membranes (blue arrows) and taken up by GEnC cells within vesicles (red arrows) after 24 h (naïve cells showed evidently empty vesicles; green arrows). The presence of the GO material persisted within cellular vesicles for up to 1 week, the latest time point of this study.

Podocytes are critical for maintaining an intact glomerular filter,[25] for that reason conditionally immortalized human podocytes[32] were exposed to GO in this study. The percentage of podocyte cell viability treated with GO at different concentrations (5, 25, 100, and 200 μg/mL) was again determined by a modified LDH assay at 24 and 48 h after treatment (Figure 5A). Significant reductions in cell viability were only detected after 48 h at high GO exposures (100 and 200 μg/mL). The effect of GO on the podocyte barrier function, as measured by ECIS (Figure 5B), shows the barrier function of podocytes pretreated with 25 μg/mL of GO 24 h before culturing on the ECIS plate, while the bottom graph demonstrates cells that were directly treated on the ECIS plate. Cells were washed after 24 h, and the media was changed every 2 days and monitored under ECIS for 1 week, the same as with the GEnC cells. When cells were pretreated, they retained normal resistance similar to naïve cells. Upon treatment with GO directly on the ECIS plate, the cells exhibited a significant reduction in resistance, that was gradually restored, reaching the naïve cell level more than 48 h after treatment. Puromycin aminonucleoside (PAN) treatment (a podocyte toxin, used as a positive control) resulted in complete reduction of resistance 24 h after treatment that indicated podocyte detachment and cell death due to apoptosis and reactive oxygen species generation, in agreement with previous reports.[33]

Human podocyte morphology was studied by immunocytochemistry staining of the cell cytoskeleton with α-tubulin and β-actin (Figures 5C and S7). Some changes in the morphology of the cells were observed, with α-tubulin and β-actin fiber contraction starting at 24 h, with complete recovery after 1 week. The cell aspect ratio exhibited a significant reduction, indicating changes in morphology at 24 h after treatment, with gradual recovery starting at 48 h until almost complete recovery was achieved after 1 week of GO exposure. The gaps between cells (Figure 5C*iii*) were also increased, confirming cell contraction, and a similar pattern of recovery was observed after 1 week. The TEM images of the podocyte cells in Figures 5D and S6B show similar interactions of GO with cell membranes (blue arrows). Uptake started earlier than GEnC cells (after 1 h of treatment). Indeed, significant amounts of GO were internalized by cells in large vesicular structures (red arrows) after 24 and 48 h. However, unlike GEnC cells the

DOI: 10.1021/acsnano.6b03358
ACS Nano 2016, 10, 10753−10767

Scheme 1. Schematic of the GFB and the four possible mechanisms by which thin, flexible GO sheets are thought to be able to trespass the different barrier components[a]

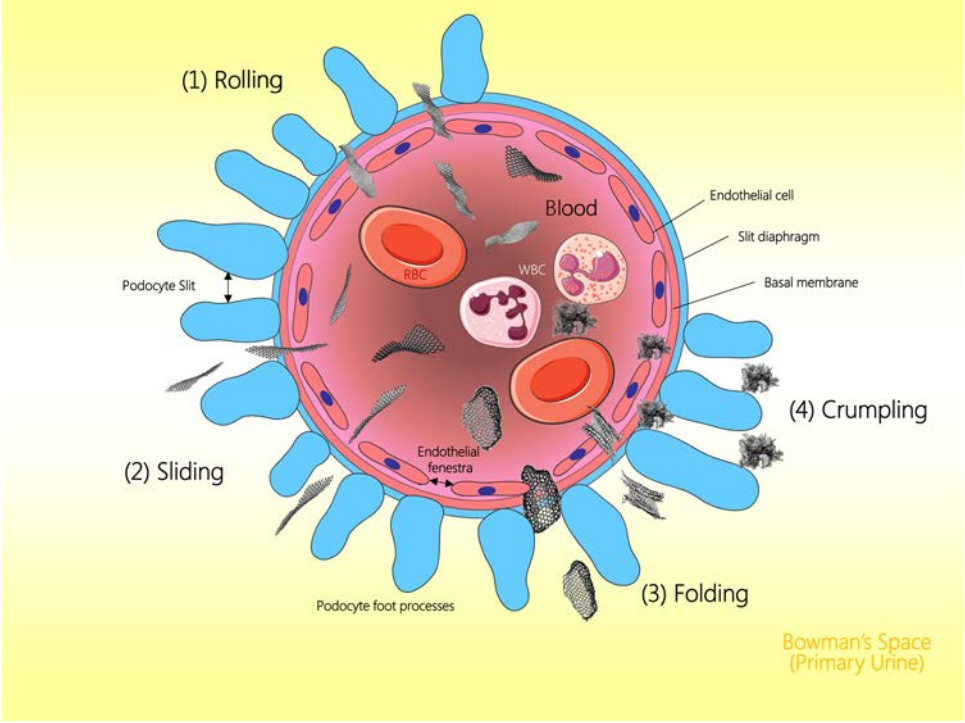

[a]RBC is red blood cells; WBC is white blood cells.

vesicles appeared empty after 1 week (green arrows), indicative of exocytotic or degradative processes.

DISCUSSION

The impact of graphene-based material exposure on tissue pathophysiology has been studied to a limited extent *in vivo*. One critical organ previously identified in a few studies is the lung, its response manifested mainly as acute inflammation and lung granulomatosis at high concentrations (>10 mg/kg).[34−38] Pulmonary accumulation of intravenously administered GO sheets in our view is mainly due to poor colloidal dispersibility of the material tested, leading to entrapment of large colloidal particulates in the immediate capillary beds they transport through, that are the lung capillaries.[15] Some hepatic adverse responses have also been reported previously.[39]

When well-dispersed GBM travel through the systemic blood compartment, they will go through the lung capillaries, where the smaller and thinner 2D sheets will begin to get excreted through the GFB in the kidney, while the thicker and larger sheets will remain in circulation and accumulate in the spleen and liver.[20] The urinary excretion of GO sheets following their administration into the systemic blood circulation has been reported previously[8,17−19] and can be attributed to their structural features (thinness), flexibility, and orientation in flow that leads to their ability to cross the GFB (Scheme 1). While faecal excretion has been reported to a lesser extent, it seems to be related to certain functionalization moieties and to route of administration. Extensive faecal excretion was reported after i.v. administration of dextran-functionalized GO,[8,40] and to a lesser extent PEGylated GO.[17] Oral administration of GO resulted in extensive faecal elimination.[16]

We have recently demonstrated that the urinary excretion of (^{64}Cu)DOTA-GO sheets (by PET/CT) critically depends on their thickness; the thicker the GO sheets, the less their capacity to pass through the GFB.[20] In the present study we confirmed the high radiolabeling stability of labeled GO *in vivo* (Figure 1C*ii*) to further validate the urinary excretion of intact GO sheets. A similar excretion pattern was obtained for the nonfunctionalized, thinner GO sheets (1−2 layers) with a clear Raman signature for GO detected in the urine as previously reported.[19] The high negative charge of 2D GO sheets (in the order of −50 mV) suggests that its filtration through the GFB may be occurring *via* a mechanism different to that reported for similarly sized, but structurally and chemically very different, positively charged dendrimers.[41]

The extraordinarily large degree of urinary excretion observed for thin, well-dispersed GO sheets required interrogation of the impact on renal function. In our study, LPS was injected as a nephrotoxic agent, and we observed acute glomerular injury as previously reported,[42−44] with elevated serum levels of creatinine, urea, and ALB. In mice treated with GO at an escalated dose regime (from 2.5 to 10 mg/kg), no significant change in serum kidney function markers (serum creatinine, urea and ALB levels) was detected. Moreover, only traces of urinary ALB were measured at the highest GO dose (10 mg/kg), but the changes were statistically insignificant after quantifying the physiologically more relevant protein:creatinine ratio. However, animals at this highest GO dosing regimen exhibited compromised weight gain (Figure 2C), therefore, the dose of 10 mg/kg was considered above the toxicity threshold and was not used in later studies for ethical and animal welfare purposes. Others have also reported that doses of 10 mg/kg or above of GO cause toxic responses in mice after i.v. administration of this material.[36,45]

Comprehensive histopathological examination of kidney sections of animals treated with GO (7.5 mg/kg) showed no

DOI: 10.1021/acsnano.6b03358
ACS Nano 2016, 10, 10753−10767

signs of increased cellularity or proliferation in any part of the glomeruli, nor were any signs of inflammation, fibrosis, necrosis, thrombosis, or damage noted. For this reason, it was not possible to follow the conventional renal pathology scoring systems.[46] Despite this, we performed detailed measurements of renal cortical thickness, number of glomeruli per whole kidney, longitudinal glomerular diameter, and glomerular cell counts. No significant changes in all these parameters were detected between GO-injected mice and the control group (dextrose-injected) up to 1 month, indicating the absence of any glomerular damage. Similarly, examination of the renal tubules indicated the normal proximal (p) tubules with normal brush border (microvilli) and normal distal (d) convoluted tubules. No dilatation, thickening, flattening, cysts and/or castes were observed up to 1 month in the tubules.

The graphene literature is somehow controversial in reporting the adverse effects in preclinical settings. This might be due to variability between materials, amounts administered, and routes of administration. Histological effects and kidney function marker alterations have been previously reported by Shang *et al.*[47] and Patlolla *et al.*,[48] however GO was administered intraperitoneally and orally in these studies. Intravenous administration of GO has also been performed by Wang *et al.*,[36] who reported mortality in 4/9 of i.v. injected mice only in the high dose treated group (20 mg/kg). This was thought to be due to airway blockage and severe histological alteration in major organs including kidney. Li *et al.*,[39] also reported changes in kidney and hepatic markers after 24 h from i.v. injection of GO (5 mg/kg) with no histopathological alterations to kidney even after 3 months. Alterations in kidney marker levels and in renal histology were observed by Sasidharan *et al.*[49] after i.v. administration of few-layer graphene materials at high doses of 20 mg/kg. In a different study, Liu *et al.* reported that repeated i.v. administration at low GO doses (0.2 and 0.3 mg/kg in 7 repeated doses over 15 days) resulted in glomerular swelling and blockage of Bowman's space.[50] Kanakia *et al.* reported proteinaceous casts in tubules and congestion within vascular spaces in the renal cortex after administration of an extremely high single dose (250 mg/kg) of dextran-functionalized GO that is above the toxicity threshold.[40] No evidence of direct excretion of graphene-based materials has been reported by any of the mentioned studies. Contrary to the above, there are numerous published reports of studies performing treatments with GO at 10 mg/kg,[45] functionalized GO up to 5 mg/kg,[19,39] and graphene quantum dots (GQD) up to 20 mg/kg[51,52] that show no damage to the kidneys of mice by histological examination. Moreover, different studies have also reported renal excretion of the GO material with no histopathological or any significant adverse effects evidenced by kidney function markers.[16−19,53]

Examination of the glomeruli cross sections using electron microscopy (Figure 3B) allowed measurement of the glomerular BM thickness, podocyte foot processes width, endothelial fenestra width, and podocyte slit size, all crucial components of a functioning GFB.[23] Kidneys were extracted at 30 min postinjection of GO, the peak time of kidney residence as determined in this study (Figure 1C), in agreement with our previous reports.[19,20] No significant changes were detected in comparison to the control group, and numerical measurements were in agreement with the standard values published in previous kidney studies.[23,54,55] This further suggested that excretion of the GO sheets occurred as a passive mechanism, with no damage to the GFB, possibly based on their morphological reconfiguration[23] either by sliding,[56] squeezing, rolling, or folding of the sheets (Scheme 1). Similarly, it has been reported previously that chemically functionalized carbon nanotubes with their longitudinal dimension exceeding the GFB cutoff were also excreted intact in the urine of injected mice; the proposed mechanism was that of passive translocation through the GFB[27,57−59] with no residual accumulation or renal damage reported.[59] We believe a similar process is taking place for thinner and more flexible GO sheets, leading to their much more substantial (in terms of % injected dose) urinary excretion.

As the GO sheets translocate through the GFB, two cellular components of this complex biological barrier are encountered, namely, the GEnC and the glomerular podocytes.[22,23] We interrogated the effects from GO exposure on these two human cell types *in vitro* at high exposure levels. The cytotoxic responses observed for both cell types appeared moderate, at high GO doses (100 and 200 μg/mL) and after 48 h of exposure. The GEnC cells appeared more sensitive than podocytes. However, the reported effects of graphene-based material on kidney cells remain scarce. Among these, the study by Sasidharan *et al.* reported that pristine graphene triggered cytotoxic responses in monkey kidney epithelial cells (Vero cells) by apoptosis created by adsorption on the membrane of the hydrophobic sheets, while the more hydrophilic oxidized graphene was internalized and appeared nontoxic to these cells at a concentration of 25 μg/mL after 24 h.[60] Similarly, De Marzi *et al.* demonstrated no cytotoxicity on Vero cells after 24 h of treatment with GO, but detected some genotoxic effects at concentrations of 100 μg/mL.[61]

Following the cytotoxicity study, we decided to focus on the impact of GO exposure to the barrier function of the two cell cultures using a subcytotoxic dose (25 μg/mL) already 100 times the expected exposure dose to the kidney *in vivo*, based on the total surface area of the rodent glomerular capillaries (~4660 cm^2)[62] and that of the cell culture well-plates we used (~9.6 cm^2). Considering that approximately 60% of the injected GO dose was excreted through the kidneys, it was estimated that the glomerular endothelium would interact with a maximum of 120 μg of GO *in vivo*, corresponding to 0.25 μg for a ~9.6 cm^2 surface area of the cell culture well plate. The barrier function of both kidney cell types was evaluated using ECIS, a technique that measures the integrity of a monolayer of cells in response to physiological agonists or pharmacological and toxicological compounds.[42,63]

Upon pretreatment of both kidney cell types with GO (at 25 μg/mL) for 24 h before culturing on the ECIS plate, the resistance of the cell barrier was moderately increased for the endothelial cells and unchanged for the podocytes (Figures 4B and 5B, respectively). This indicated that the cells were still viable and adherent, with an intact barrier even after their handling (trypsin treatment, detachment, washing, and reculturing on the ECIS plate). Although both cells seemed to have internalized the GO sheets to a similar extent after 24 h, the differences observed in cell barrier resistance can be attributed to the way the two cells types responded to the material in a different manner at longer time points. The increased resistance observed in GEnC cells could be due to the prolonged retention of the GO sheets even after 1 week of treatment (Figure 4D). On the other hand, podocytes appeared to interact with GO more avidly and, more importantly, seemed capable of removing the internalized material (presumably by exocytosis) (Figure 5D). Podocytes are indeed reported to be

DOI: 10.1021/acsnano.6b03358
ACS Nano 2016, 10, 10753−10767

active phagocytic cells, with a key role in the constant removal of debris from the GFB.[64,65]

The reduction in cell barrier resistance a few hours after the direct exposure to GO on the ECIS plate could be due to the temporary loss of the cell−cell interactions due to cell motility and contraction in response to the GO. Resistance reverted back to normal levels at later time points. This was consistent with the observed changes in cell morphology (cell contraction) and creation of gaps between the cultured cells detected only after 24 and 48 h of GO exposure, illustrated by staining the cell bodies with α-tubulin and β-actin. Endothelial cells have been shown to contract under the influence of certain mediators that lead to intercellular gap formation.[66] On the other hand, podocytes are highly polarized cells, characterized by a dynamic actin-based cytoskeleton and small actin-based foot processes that can be rapidly remodeled upon exposure to toxins.[67] These known differences can explain the steeper decrease in cell barrier resistance detected in the case of podocytes after 24 h. Previous studies that evaluated cytotoxic responses to graphene-based material exposure by ECIS using insect cells[68] and HeLa cells[69] report an adequate cell adherence indicative of biocompatibility. To the best of our knowledge, the use of ECIS to determine the barrier function of human kidney cells in response to graphene-based materials has not been previously reported.

Lastly, we sought to investigate the responses to high GO doses of these two types of specialized human kidney cells by electron microscopy of cell sections. Significant amounts of GO sheets were internalized by both cell types after 24 and 48 h (Figures 4D, 5D, and S6). The GO material was seen stacking within large intracellular vesicles (red arrows) in both cell types, indicating an effective phagocytic mechanism. This mechanism of cellular uptake has been observed by others using GO and different cell types.[56,70,71] Cell membranes were structurally intact, with no membrane damage observed (also in agreement with the absence of LDH release and absence of trypan blue uptake). Plasma membrane damage has been reported by others using thick (*i.e.*, much more rigid), large (multiple microns in lateral dimension) pristine graphene platelets with sharp irregular edges.[72,73] We do not believe such observations are relevant to small, thin, well-oxidized GO sheets as those used in this study. Interestingly, the 2D sheets had different orientations when interacting with cell membranes, but most positioned perpendicular to the membrane axis, presumably further facilitating phagocytic internalization. The more rapid uptake and subsequent release of GO sheets by the podocyte cells herein, compared to the endothelial cells, is due to their higher phagocytic activity and cellular motility.[67] This agrees with the preservation of their principal function in releasing captured material into the primary urine compartment (Bowman's space).

CONCLUSION

The extraordinary levels of urinary excretion observed following i.v. administration of thin, well-dispersed GO sheets did not cause any significant change in kidney function or structural damage to the glomerular and tubular regions of the kidneys up to 1 month postinjection at escalating doses. The interaction of GO sheets with cultures of endothelial cells and podocytes that form cellular components of the renal filtration system indicated that the cells can regain their barrier function rapidly following exposure, even at unrealistically high GO exposures. Both cell types were able to internalize the GO material without any significant or irreversible adverse reactions. This study provides initial evidence of the interaction between the renal barrier and its responses to intravenously administered thin (1−2 nm) GO sheets of lateral dimensions largely below 1 μm. More broadly, it offers an understanding of the mechanisms by which 2D materials may interact with physiological barriers (such as the GFB) in view of their potential diagnostic and therapeutic utilization.

EXPERIMENTAL SECTION

Synthesis, Functionalization, And Radiolabeling of GO. GO was prepared from flake graphite (Barnwell), by the modified Hummers' method,[28] and functionalized with DOTA as published previously.[19] Thorough characterization of the thin GO material used in these studies has been reported to indicate that for radiolabeling, GO-DOTA was diluted with an equal volume of 0.2 M ammonium acetate buffer at pH 5.5, then 2−20 MBq as $^{111}InCl_3$ was added. The indium was left to react with the GO-DOTA for 60 min at 60 °C, after which the reaction was stopped by the addition of 0.1 M EDTA chelating solution; this was followed by the removal of the free unattached EDTA[^{111}In] by centrifugation. The purity of the final product was determined by taking an aliquot of the final product and then diluting it 5-fold in phosphate-buffered saline (PBS). Next, 1 μL was spotted on silica gel-impregnated glass fiber sheets (PALL Life Sciences, U.K.). The strips were developed with a mobile phase of 50 mM EDTA in 0.1 M ammonium acetate and allowed to dry before stating the analysis. This was then developed, and the autoradioactivity was counted using a cyclone phosphor detector (Packard Biosciences, U.K.). The immobile spot on the TLC strips indicated the radiolabeled material, while free EDTA[^{111}In] was seen as the mobile spot near the solvent front. This was repeated until no further mobile spot was determined near the solvent front, indicating no free EDTA[^{111}In] before injecting the material in mice.

Atomic Force Microscopy. A Bruker Multimode 8 was used in tapping-mode with an J-type scanner, Nanoscope VI controller, Nanoscope v614r1 control software (Veeco, Cambridge, U.K.) and a silicon tapping tip (NSG01, NTI-Europe, Apeldoorn, The Netherlands) of 10 nm curvature radius, mounted on a tapping mode silicon cantilever with a typical resonance frequency 283−374 kHz and a force constant of 12−103 N/m (Bruker OTESPA, U.K.). Images were taken in air, by depositing 40 μL of the sample on a freshly cleaved mica surface (Agar Scientific, Essex, U.K.) coated with poly-L-lysine 0.01% (Sigma-Aldrich, U.K.) and allowed to adsorb for 2 min. Excess unbound material was removed by washing with Milli-Q H_2O and then drying in air; this step was repeated once. Size distributions were carried out using ImageJ software to measure the lateral dimension of individual graphene sheets, by counting more than 100 sheets. Sheet thickness was determined from the AFM height profiles.

Zeta Potential Measurements. Electrophoretic mobility (μ) was measured by Malvern Zetasizer Nano ZS (U.K.) after dilution of samples with Milli-Q H_2O in disposable Zetasizer cuvettes (Malvern Instruments, U.K.). Default instrument settings and automatic analysis were used for all measurements, where μ was converted automatically by the equipment software to zeta potential (ζ) values since it is directly related to zeta potential by Henry's equation.[74] All values for samples prepared are triplicate measurements, and values were expressed as mean ± SD.

Raman Spectroscopy of GO in Solution and GO in Urine. Raman spectra of samples were recorded after drop casting samples on glass slides and evaporating the solvent. Measurements were carried out using a 50× objective at λ = 633 nm laser excitation and 0.4 mW power, by using a DXR Raman microscope (Thermo Scientific, U.K.). An average of at least five different locations within each sample was measured.

Animal Handling Procedures. Eight week-old C57BL/6 mice (18.1 ± 0.7 g) were obtained from Harlan (Oxfordshire, U.K.), allowed to acclimatize for 1 week, and kept under a 12 h light/dark cycle under steady temperature and humidity with access to food and water ad libitum for the duration of the experiments. All experiments

DOI: 10.1021/acsnano.6b03358
ACS Nano 2016, 10, 10753−10767

were conducted with prior approval from the U.K. home office. Mice were injected with GO solutions in dextrose 5% (2.5, 5, and 10 mg/kg) and Dex 5% (negative control), and then different experiments below were conducted at 24 h and 1 month. LPS 5 mg/kg at 24 h was used as the positive control. These mice were only kept for 24 h, as the mice showed symptoms of distress, and were culled after 24 h, in accordance with U.K. home office guidance. The mice were continuously monitored and examined during experiments and were weighed every 4 days.

Single Photon Emission Computed Tomography (SPECT/CT) Imaging. The mice were anaesthetised by isofluorane inhalation. Mice were injected *via* the tail vein with 200 μL containing 50 μg (2.5 mg/kg) of (^{111}In)GO-DOTA with approximately 5−6 MBq of radioactivity. Immediately after the injection (t = 0−1 h), images of the mice were obtained using the Nano-SPECT/CT scanner (Bioscan, USA). SPECT images were obtained in 24 projections over 40−60 min using a four-head scanner with 1.4 mm pinhole collimators. CT scans were taken at the end of each SPECT acquisition, and all images were reconstructed with MEDISO software (Medical Imaging Systems). Fusion of SPECT and CT images was carried out using the PMOD software.

***In Vivo* Stability of (^{111}In)GO-DOTA.** The *in vivo* radiolabeling stability of the (^{111}In)GO-DOTA sample was determined by performing TLC analysis of the urine samples of injected mice and comparing them to the samples prepared before injection. Then, 1 μL of each sample was spotted on a silica gel impregnated glass fiber sheets (PALL Life Sciences, U.K.). The strips were developed with a mobile phase of 25 mM EDTA in 0.1 M ammonium acetate and allowed to dry before analysis. This was then developed, and the autoradioactivity counted using a Fujifilm fluorescence image analyzer (FLA-3000 series, Tokyo, Japan).

Quantification of the Total Amount of (^{111}In)GO-DOTA Excreted. Urine of injected mice was extracted by direct bladder puncture 2 h after the injection of 200 μL containing 50 μg (2.5 mg/kg) of (^{111}In)GO-DOTA or (^{111}In)EDTA, with approximately 0.5−1 MBq of radioactivity. Mice that were under terminal aesthesia underwent surgery and urine extraction directly from the bladders by 1 mL disposable insulin syringes; this approach was used to minimize the loss of sample, as would be case with other methods of collection.[75] Furthermore, kidneys and bladders were extracted at the same time to detect the total amounts excreted. The radiation from each urine, kidney, and bladder was counted on a gamma counter (PerkinElmer, U.S.A.), together with a dilution of the injected dose, with dead time limit below 60%. Then, the total amount excreted was calculated as the sum of urine, kidney, and bladder counts and then determined as percentage of the total amount calculated for the control sample (^{111}In)EDTA. This expression gives a more accurate estimation of total quantities excreted because chelating agents will be excreted almost entirely with minimal tissue accumulation.[75]

Serum Kidney Function Analysis. Blood was collected from mice after 24 h or 1 month of injection of GO at different concentrations (2.5, 5, and 10 mg/kg of Dex 5% or 24 h after injection of LPS (5 mg/mL) by cardiac puncture and left to coagulate at room temperature for 30−45 min. The samples were then centrifuged at 1000−2000 g for 10 min using a refrigerated centrifuge. Serum was carefully separated and frozen at −20 °C until further analysis. The serum samples (4−8 mice per group) were sent to the Laboratory Diagnostic Service of the Royal Veterinary College (London, U.K.) for analyzing the levels of creatinine, urea, and ALB. Values are expressed as mean ± SE (n = 4−8 mice).

Urine Protein Analysis. Urine samples were collected by the spot urine collection method[75] after 24 h or 1 month of injection of GO at different concentrations (2.5, 5, and 10 mg/kg), Dex 5% or 24 h after LPS 5 mg/mL and then refrigerated until further analysis. Then, 10 μL of each urine sample was mixed with Protein Solving Buffer (Fisher Scientific, U.K.) for a final volume of 20 μL and boiled for 5 min at 90 °C. Samples were then loaded in 4−20% Precise Tris-HEPES Protein Gel (Thermo Scientific, U.K.). The gel was run for 50 min at 150 V for 50 times in diluted Tris-HEPES SDS Buffer (Thermo Scientific, U.K.) running buffer. The gel was then stained with EZ Blue Gel Staining reagent (Sigma Life Science, U.K.) overnight followed by washing in distilled water for 2 h. Urine samples (50 μL of each, 4−8 mice per group) were sent to the Laboratory Diagnostic Service of the Royal Veterinary College (London, U.K.) for analyzing the protein:creatinine ratio. Values were expressed as mean ± SE (n = 4−8 mice).

Kidney Histopathological Analysis. Kidneys of mice injected with GO (7.5 mg/kg) and control Dex 5% were extracted after 24 h and 1 month of injections and then fixed with 4% paraformaldehyde, followed by paraffin embedding. Sections of 5 μm were cut and stained with H&E, and images were collected using a 20× objective and 3D Histech Pannoramic 250 Flash slide scanner. Images were processed and analyzed using Pannoramic Viewer (http://www.3dhistech.com/) and Fiji/ImageJ software (version 1.5c; National Institutes of Health, Bethesda, MD). The histopathological examination of kidney glomeruli and tubules and quantitative analysis were performed as per previous reports.[21,46,76−81] The total number of nuclei and size as well as the longitudinal diameter of each glomerulus were calculated for at least 50 glomeruli from several random kidney sections for each mouse. The total number of glomeruli per whole kidney was determined by multiplying the average number of glomeruli per kidney section (counted from several random kidney sections) by 50 (this is the total number of slices containing one whole glomerulus with an average diameter of 50 μm). The cortical thickness was calculated from measuring the distance between the renal capsule and the cortical-medullary junction. Values are expressed as mean ± SE (n = at least 2 mice per condition).

Kidney Ultrastructural Examination. The kidney glomerular ultrastructure was examined using TEM and STEM. Kidney tissue samples were fixed for at least 1 h in a mixture of 4% formaldehyde and 2.5% glutaraldehyde in 0.1 M Hepes buffer (pH 7.2). The samples were postfixed with 1% osmium tetroxide and 1.5% potassium ferrocyanide in 0.1 M cacodylate buffer (pH 7.2) for 1 h, then in 1% uranyl acetate in water for another hour. The specimens were dehydrated with increasing concentrations of ethanol and then acetone. The samples were subsequently infiltrated with TAAB 812 resin and polymerized for 24 h at 60 °C. Ultrathin 70 nm thick sections were cut with a Reichert Ultracut ultramicrotome and placed on Formvar/carbon-coated slot grids (EMS, U.S.A.). The grids were observed in a Tecnai 12 Biotwin TEM at 100 kV accelerating voltage. Images were taken with Gatan Orius SC1000 CCD camera. STEM images were acquired on a FEI Titan 80/200 ChemiSTEM equipped with a probe-side aberration corrector and a FEI Talos, both operating at an acceleration voltage of 200 kV and using an X-FEG source. During STEM imaging, two images were simultaneously acquired: the bright field (BF) image, which exhibits contrast similar to the phase-contrast TEM imaging, and the high angle annular dark field (HAADF) image, which contains mass−thickness information, *i.e.*, the measured signal scales the thickness and the density of the specimen. The contrast of the HAADF image was usually higher than that of BF/phase-contrast TEM images and allowed better identification of the structure in the specimen.[82] For STEM imaging, the beam current was set to 75 pA, and the pixel time ranged between 10 and 20 μs. The collection angles of the BF and HAADF detectors were 0−11 mrad and 48−190 mrad, respectively. Ultrastructural morphometry analysis was carried out according to references.[54,83] Glomerular BM thickness, podocyte foot process width, podocyte slit size, and endothelial cell fenestra size were quantified using Fiji/ImageJ software (version 1.5c; National Institutes of Health, Bethesda, MD). This was done by analyzing 7−10 regions per observation and is reported as mean ± SE (n = at least 2 mice per condition).

Cell Cultures. Kidney cells were cultured as described before.[84,85] These were derived by incorporating a temperature-sensitive SV40 gene that enables cells to proliferate at the permissive temperature (33 °C) and to differentiate at the nonpermissive temperature (37 °C). The conditionally immortalized human GEnC[30] and human podocytes[32] were grown in monoculture in uncoated tissue culture plates. GEnC were grown in endothelial basal medium-2 (CC-3156; Lonza, Slough, U.K.) containing 5% (v/v) FCS and EGM-2 BulletKit growth factors (CC-4147; Lonza), except vascular endothelial growth factor. Podocytes were cultured in RPMI-1640 medium with

DOI: 10.1021/acsnano.6b03358
ACS Nano 2016, 10, 10753−10767

glutamine (R-8758; Sigma-Aldrich) supplemented with 10% (v/v) FCS (Life Technologies) and 5% (v/v) insulin, transferrin, and selenium (ITS) (I-1184; Sigma; 1 mL/100 mL). Both cells were grown until 70−80% confluency at 33 °C. The GEnC were then thermo-switched to 37 °C for 5 days, while the podocytes were thermo-switched to 37 °C for 14 days before all experiments. The GEnC were seeded at 100,000 cells/cm^2,[85] while podocytes were seeded at 60,000 cells/cm^2 in wells of different sizes depending on the experiment.

Modified Lactate Dehydrogenase Cytotoxicity Assay. GEnC and podocyte cells were plated in 96-well plates and left to adhere overnight. The cells were then incubated with GO at different concentrations (0−200 μg/mL) in complete media. Untreated cells cultured in free medium and cells treated with DMSO 10% were taken as controls. In addition, thrombin and PAN were used as additional controls for GEnC and podocytes, respectively. A modified LDH assay was used to avoid interference related to the autofluorescence of GO itself. The LDH leakage was assessed in the survived cells, rather than the LDH released in the media upon GO induced-cell death. Therefore, the media containing dead cells was aspirated, and the intact cells were lysed with 10 μL of lysis buffer (0.9% Triton X100) mixed with 100 μL of media, for 45−60 min at 37 °C to obtain a cell lysate which was then centrifuged at 1500 rpm for 5 min in order to pellet down the GO. Fifty μL of the supernatant of the cell lysate was mixed with 50 μL of LDH substrate mix in a new microtiter plate and incubated for 15 min at room temperature. Absorbance was read at 490 nm using a plate reader. The amount of LDH detected represented the number of live cells which survived the treatment. The percentage cell survival was calculated using the following equation:

$$\text{percentage cell survival} = A_{490\text{nm}}\text{of treated cells}/A_{490\text{nm}}\text{of untreated cells} \times 100$$

Trypan Blue Cell Exclusion Assay. Trypan blue assay was carried out to determine the cell mortality. GEnC and podocyte cells were plated in 12-well plates and left to adhere overnight. The cells were then incubated with GO at different concentrations (0−200 μg/mL) in complete media. Untreated cells cultured in free medium and DMSO 10% treated cells were taken as controls. In addition, thrombin and PAN were used as additional controls for GEnC and podocytes, respectively. Twenty-four and 48 h later, the supernatants were collected, and the cells were detached with 300 μL trypsin-EDTA solution. The mixture of the supernatant and detached cells was centrifuged at 1500 rpm for 5 min. Then cells were redispersed in complete media, and an equal volume of Trypan blue solution was added. After staining for 5 min, the cells were counted using a cytometer. The dead cells were stained in blue. The percentage cell mortality was counted from the following equation:

$$\text{percentage cell mortality} = \text{dead cell count}/\text{total cell count} \times 100$$

Electric Cell−Substrate Impedance Sensing Assay. The function of the kidney cells was evaluated using electrical cell−substrate impedance sensing (ECIS ZO, Applied Biophysics); this technique involves the investigation of the barrier quality of adherent confluent cell monolayers (this is the main function of the kidney cells). This was carried out by passing an electric current at low frequency (4000 Hz). Cell resistance was determined by the ability of the cells and their cell−cell and cell−matrix to block the electric flow.[31] Failure to resist the current, characterized by reduced resistance, indicates an impairment to the barrier quality and indicates failure of cell−cell interaction and creation of huge gaps between cells. Complete medium for both GEnC cells and podocytes was equilibrated to match the CO_2 levels (5%) and temperature (37 °C) of the experiment for 3 h. ECIS array wells (8W10E, ibidi GmbH) were coated with 10 mM cysteine solution and washed three times with sterile H_2O. Arrays were subsequently coated with the protein of choice (collagen) diluted in sterile NaCl (150 mM) for 1 h at room temperature. Equilibrated medium was then added to coated wells, and the arrays were calibrated using test cards. Cells were trypsinised as normal and resuspended in equilibrated medium. Cells (either untreated or already treated) were then seeded on each well of the array, left to adhere to the ECIS wells overnight, and treated the next day accordingly. The day after treatment, cells were washed with media, and the media was changed every 2 days. Data were acquired at a single frequency (4000 Hz).

Immunocytochemistry and Cell Image Analysis. GEnC and podocytes were plated on glass coverslips in 24-well plates and left to adhere overnight; the cells were then treated accordingly. The day after treatment, cells were washed with media, and the media was replaced every 2 days. At different time points after treatment (1 h, 24 h, 48 h, and 1 week), the cells were washed with PBS and fixed with 4% paraformaldehyde for 15 min at room temperature. This was followed by ice-cold methanol permeabilization for 5 min at −20 °C, followed by washing with PBS three times. The cells were then blocked for 1 h with 5% normal goat serum and 0.3% Triton in PBS. They were then incubated overnight at 4 °C with either α-tubulin (Sigma, no. T9026) or β-actin (Cell Signaling, no. 4970, 13E5 rabbit mAb). The next day, they were washed with PBS three times and incubated with the fluorochorome-conjugated secondary antibodies (antimouse-Cy3 and antirabbit-Cy3, respectively) for 1−2 h at room temperature and then washed three times with PBS. The coverslips were then mounted with Prolong Gold Anti-Fade Reagent with DAPI (Cell signaling, no. 8961) and left to dry at room temperature. Images were then captured using a Zeiss Axio Observer epi-fluorescence microscope. Both α-tubulin and β-actin were excited in the Cy3 channel (550 nm excitation and 570 nm emission) since they were performed in separate experiments. DAPI channel was used for the nuclear counter stain (350 nm excitation and 470 nm emission). All images were analyzed using the built-in Axiovision software. For the quantitative analysis of cell morphology and cell gap formation, Fiji/ImageJ software (version 1.5c; National Institutes of Health, Bethesda, MD) was used. The cell shape change depended on determining the aspect ratio of cells from dividing the maximum diameter of the cell by the minimum diameter of the cell.[37,86] The cell gaps were obtained by setting a color threshold and choosing the best fit.

Ultrastructural Examination of Kidney Cells. Both GEnC and podocytes were examined using TEM. The cells were plated on aclar and fixed for at least 1 h in a mixture of 4% formaldehyde and 2.5% glutaraldehyde in 0.1 M Hepes buffer (pH 7.2). Then, they were postfixed with 1% osmium tetroxide and 1.5% potassium ferrocyanide in 0.1 M cacodylate buffer (pH 7.2) for 1 h and then in 1% uranyl acetate in water for another 1 h . The specimens were dehydrated with increasing concentrations of ethanol and then acetone. Samples were subsequently infiltrated with TAAB 812 hard resin and polymerized for 24 h at 60 °C. Ultrathin 70 nm sections were cut with a Reichert Ultracut ultramicrotome and placed on Formvar/carbon-coated slot grids (EMS, U.S.A.). The grids were observed in a Tecnai 12 Biotwin TEM at 100 kV accelerating voltage. Images were captured with Gatan Orius SC1000 CCD camera.

Statistical Analysis. The results of all animal experiments are represented as mean ± standard error (SE), while the results of cellular experiments are represented as mean ± standard deviation (SD). Statistical significance was carried out using one-way ANOVA with Tukey's *posthoc* test when considering multiple comparisons, by using IBM SPSS statistics 22 software. The Student's t test was considered for the ultrastructural quantitative analysis of the kidney glomerular TEM images involving glomeruli BM thickness, podocyte foot processes width, endothelial fenestra width, and podocyte slit size since they did not involve multiple comparisons.

ASSOCIATED CONTENT

Supporting Information

The Supporting Information is available free of charge on the ACS Publications website at DOI: 10.1021/acsnano.6b03358.

Supporting Figures S1−S7 (PDF)

DOI: 10.1021/acsnano.6b03358
ACS Nano 2016, 10, 10753−10767

AUTHOR INFORMATION

Corresponding Authors

*E-mail: rachel.lennon@manchester.ac.uk.
*E-mail: kostas.kostarelos@manchester.ac.uk.

Notes

The authors declare no competing financial interest.

ACKNOWLEDGMENTS

This work was partially supported by the EU 7th RTD Framework Programme, Graphene Flagship project (FP7-ICT-2013-FET-F-604391). The authors would like to acknowledge CNRS and the staff in the Faculty of Life Sciences EM Facility for their assistance and the Wellcome Trust for equipment grant support to the EM Facility. The University of Manchester Bioimaging Facility microscopes used in this study were purchased with grants from the BBSRC, Wellcome Trust, and the University of Manchester Strategic Fund. E.P. and S.H. would like to acknowledge funding from the Engineering and Physical Sciences Council (EPSRC) U.K. Grants EP/K016946/1 and EP/M010619/1 and Defence Threat Reduction Agency Grant HDTRA1-12-1-0013. The authors wish to acknowledge Mr. R. Meadows from the Bioimaging Facility. The authors are also thankful to Mr. P. Walker from the Histology Facility, University of Manchester for his advice and assistance in the tissue histology. The authors also wish to thank Dr. N. Hodson from the Bio-AFM Facility (Centre for Tissue Injury and Repair at the University of Manchester) for assistance and advice regarding the AFM instrumentation. The authors are also thankful to M. J. Randles from the Wellcome Trust Centre for Cell-Matrix Research, Faculty of Life Sciences, and University of Manchester for assistance and advice with the ECIS instrumentation.

REFERENCES

(1) Geim, A. K. Graphene: Status and Prospects. *Science* **2009**, *324*, 1530−1534.
(2) Novoselov, K. S. Nobel lecture: Graphene: Materials in the Flatland. *Rev. Mod. Phys.* **2011**, *83*, 837−849.
(3) Novoselov, K. S.; Falko, V. I.; Colombo, L.; Gellert, P. R.; Schwab, M. G.; Kim, K. A Roadmap for Graphene. *Nature* **2012**, *490*, 192−200.
(4) Kostarelos, K.; Novoselov, K. S. Graphene Devices for Life. *Nat. Nanotechnol.* **2014**, *9*, 744−745.
(5) Kostarelos, K.; Novoselov, K. S. Exploring the Interface of Graphene and Biology. *Science* **2014**, *344*, 261−263.
(6) Shen, H.; Zhang, L.; Liu, M.; Zhang, Z. Biomedical Applications of Graphene. *Theranostics* **2012**, *2*, 283−294.
(7) Loh, K. P.; Bao, Q.; Eda, G.; Chhowalla, M. Graphene Oxide as a Chemically Tunable Platform for Optical Applications. *Nat. Chem.* **2010**, *2*, 1015−1024.
(8) Zhang, S.; Yang, K.; Feng, L.; Liu, Z. *In Vitro* and *In Vivo* Behaviors of Dextran Functionalized Graphene. *Carbon* **2011**, *49*, 4040−4049.
(9) Ferrari, A. C.; Meyer, J. C.; Scardaci, V.; Casiraghi, C.; Lazzeri, M.; Mauri, F.; Piscanec, S.; Jiang, D.; Novoselov, K. S.; Roth, S.; Geim, A. K. Raman Spectrum of Graphene and Graphene Layers. *Phys. Rev. Lett.* **2006**, *97*, 187401.
(10) Bendali, A.; Hess, L. H.; Seifert, M.; Forster, V.; Stephan, A.-F.; Garrido, J. A.; Picaud, S. Purified Neurons Can Survive on Peptide-Free Graphene Layers. *Adv. Healthcare Mater.* **2013**, *2*, 929−933.
(11) Liu, Y.; Dong, X.; Chen, P. Biological and Chemical Sensors Based on Graphene Materials. *Chem. Soc. Rev.* **2012**, *41*, 2283−2307.
(12) Servant, A.; Leon, V.; Jasim, D.; Methven, L.; Limousin, P.; Fernandez-Pacheco, E. V.; Prato, M.; Kostarelos, K. Graphene-Based Electroresponsive Scaffolds as Polymeric Implants for On-Demand Drug Delivery. *Adv. Healthcare Mater.* **2014**, *3*, 1334−1343.
(13) Pan, Y.; Sahoo, N. G.; Li, L. The Application of Graphene Oxide in Drug Delivery. *Expert Opin. Drug Delivery* **2012**, *9*, 1365−1376.
(14) Servant, A.; Bianco, A.; Prato, M.; Kostarelos, K. Graphene for Multi-Functional Synthetic Biology: The Last 'Zeitgeist' in Nanomedicine. *Bioorg. Med. Chem. Lett.* **2014**, *24*, 1638−1649.
(15) Bussy, C.; Jasim, D. A.; Lozano, N.; Terry, D.; Kostarelos, K. The Current Graphene Safety Landscape - A Literature Mmining Exercise. *Nanoscale* **2015**, *7*, 6432−6435.
(16) Yang, K.; Gong, H.; Shi, X.; Wan, J.; Zhang, Y.; Liu, Z. *In Vivo* Biodistribution and Toxicology of Functionalized Nano-Graphene Oxide in Mice After Oral and Intraperitoneal Administration. *Biomaterials* **2013**, *34*, 2787−2795.
(17) Yang, K.; Wan, J.; Zhang, S.; Zhang, Y.; Lee, S.-T.; Liu, Z. *In Vivo* Pharmacokinetics, Long-Term Biodistribution, and Toxicology of PEGylated Graphene in Mice. *ACS Nano* **2011**, *5*, 516−522.
(18) Yang, K.; Zhang, S.; Zhang, G.; Sun, X.; Lee, S.-T.; Liu, Z. Graphene in Mice: Ultrahigh *In Vivo* Tumor Uptake and Efficient Photothermal Therapy. *Nano Lett.* **2010**, *10*, 3318−3323.
(19) Jasim, D. A.; Ménard-Moyon, C.; Begin, D.; Bianco, A.; Kostarelos, K. Tissue Distribution and Urinary Excretion of Intravenously Administered Chemically Functionalized Graphene Oxide Sheets. *Chem. Sci.* **2015**, *6*, 3952−3964.
(20) Jasim, D. A.; Boutin, H.; Fairclough, M.; Ménard-Moyon, C.; Prenant, C.; Bianco, A.; Kostarelos, K. Thickness of Functionalized Graphene Oxide Sheets Plays Critical Role in Tissue Accumulation and Urinary Excretion: a Pilot PET/CT Study. *Appl. Mater. Today* **2016**, *4*, 24.
(21) Zheng, Z.; Schmidt-Ott, K. M.; Chua, S.; Foster, K. A.; Frankel, R. Z.; Pavlidis, P.; Barasch, J.; D'Agati, V. D.; Gharavi, A. G. A Mendelian Locus on Chromosome 16 Determines Susceptibility to Doxorubicin Nephropathy in the Mouse. *Proc. Natl. Acad. Sci. U. S. A.* **2005**, *102*, 2502−2507.
(22) Singh, A.; Satchell, S. C.; Neal, C. R.; McKenzie, E. A.; Tooke, J. E.; Mathieson, P. W. Glomerular Endothelial Glycocalyx Constitutes a Barrier to Protein Permeability. *J. Am. Soc. Nephrol.* **2007**, *18*, 2885−2893.
(23) Haraldsson, B.; Nystrom, J.; Deen, W. M. Properties of the Glomerular Barrier and Mechanisms of Proteinuria. *Physiol. Rev.* **2008**, *88*, 451−487.
(24) Savage, C. O. S. The Biology of the Glomerulus: Endothelial Cells. *Kidney Int.* **1994**, *45*, 314−319.
(25) Pavenstadt, H.; Kriz, W.; Kretzler, M. Cell Biology of the Glomerular Podocyte. *Physiol. Rev.* **2003**, *83*, 253−307.
(26) Lennon, R.; Byron, A.; Humphries, J. D.; Randles, M. J.; Carisey, A.; Murphy, S.; Knight, D.; Brenchley, P. E.; Zent, R.; Humphries, M. J. Global Analysis Reveals The Complexity of the Human Glomerular Extracellular Matrix. *J. Am. Soc. Nephrol.* **2014**, *25*, 939−951.
(27) Lacerda, L.; Soundararajan, A.; Singh, R.; Pastorin, G.; Al-Jamal, K. T.; Turton, J.; Frederik, P.; Herrero, M. A.; Li, S.; Bao, A.; Emfietzoglou, D.; Mather, S.; Phillips, W. T.; Prato, M.; Bianco, A.; Goins, B.; Kostarelos, K. Dynamic Imaging of Functionalized Multi-Walled Carbon Nanotube Systemic Circulation and Urinary Excretion. *Adv. Mater.* **2008**, *20*, 225−230.
(28) Jasim, D. A.; Lozano, N.; Kostarelos, K. Synthesis of Few-Layered, High-Purity Graphene Oxide Sheets from Different Graphite Sources for Biology. *2D Mater.* **2016**, *3*, 014006.
(29) Ferrari, A. C. Raman Spectroscopy of Graphene and Graphite: Disorder, Electron−Phonon Coupling, Doping and Nonadiabatic Effects. *Solid State Commun.* **2007**, *143*, 47−57.
(30) Satchell, S. C.; Tasman, C. H.; Singh, A.; Ni, L.; Geelen, J.; von Ruhland, C. J.; O'Hare, M. J.; Saleem, M. A.; van den Heuvel, L. P.; Mathieson, P. W. Conditionally Immortalized Human Glomerular Endothelial Cells Expressing Fenestrations in Response to VEGF. *Kidney Int.* **2006**, *69*, 1633−1640.
(31) Szulcek, R.; Bogaard, H. J.; van Nieuw Amerongen, G. P. Electric Cell-Substrate Impedance Sensing for the Quantification of

DOI: 10.1021/acsnano.6b03358
ACS Nano 2016, 10, 10753−10767

Endothelial Proliferation, Barrier Function, and Motility. *J. Visualized Exp.* **2014**, 51300.
(32) Saleem, M. A.; O'Hare, M. J.; Reiser, J.; Coward, R. J.; Inward, C. D.; Farren, T.; Xing, C. Y.; Ni, L.; Mathieson, P. W.; Mundel, P. A Conditionally Immortalized Human Podocyte Cell Line Demonstrating Nephrin and Podocin Expression. *J. Am. Soc. Nephrol.* **2002**, *13*, 630−638.
(33) Marshall, C. B.; Pippin, J. W.; Krofft, R. D.; Shankland, S. J. Puromycin Aminonucleoside Induces Oxidant-Dependent DNA Damage in Podocytes *In Vitro* and *In Vivo*. *Kidney Int.* **2006**, *70*, 1962−1973.
(34) Duch, M. C.; Budinger, G. R. S.; Liang, Y. T.; Soberanes, S.; Urich, D.; Chiarella, S. E.; Campochiaro, L. A.; Gonzalez, A.; Chandel, N. S.; Hersam, M. C.; Mutlu, G. M. Minimizing Oxidation and Stable Nanoscale Dispersion Improves the Biocompatibility of Graphene in the Lung. *Nano Lett.* **2011**, *11*, 5201−5207.
(35) Ma-Hock, L.; Treumann, S.; Strauss, V.; Brill, S.; Luizi, F.; Mertler, M.; Wiench, K.; Gamer, A. O.; Van Ravenzwaay, B.; Landsiedel, R. Inhalation Toxicity of Multiwall Carbon Nanotubes in Rats Exposed for 3 Months. *Toxicol. Sci.* **2009**, *112*, 468.
(36) Wang, K.; Ruan, J.; Song, H.; Zhang, J.; Wo, Y.; Guo, S.; Cui, D. Biocompatibility of Graphene Oxide. *Nanoscale Res. Lett.* **2010**, *6*, 8.
(37) Fierro-González, J. C.; White, M. D.; Silva, J. C.; Plachta, N. Cadherin-Dependent Filopodia Control Preimplantation Embryo Compaction. *Nat. Cell Biol.* **2013**, *15*, 1424−1433.
(38) Li, B.; Yang, J.; Huang, Q.; Zhang, Y.; Peng, C.; Zhang, Y.; He, Y.; Shi, J.; Li, W.; Hu, J.; Fan, C. Biodistribution and Pulmonary Toxicity of Intratracheally Instilled Graphene Oxide in Mice. *NPG Asia Mater.* **2013**, *5*, e44.
(39) Li, B.; Zhang, X. Y.; Yang, J. Z.; Zhang, Y. J.; Li, W. X.; Fan, C. H.; Huang, Q. Influence of Polyethylene Glycol Coating on Biodistribution and Toxicity of Nanoscale Graphene Oxide in Mice After Intravenous Injection. *Int. J. Nanomed.* **2014**, *9*, 4697−4707.
(40) Kanakia, S.; Toussaint, J. D.; Mullick Chowdhury, S.; Tembulkar, T.; Lee, S.; Jiang, Y. P.; Lin, R. Z.; Shroyer, K. R.; Moore, W.; Sitharaman, B. Dose Ranging, Expanded Acute Toxicity and Safety Pharmacology Studies for Intravenously Administered Functionalized Graphene Nanoparticle Formulations. *Biomaterials* **2014**, *35*, 7022−7031.
(41) Longmire, M.; Choyke, P. L.; Kobayashi, H. Clearance Properties of Nano-Sized Particles and Molecules as Imaging Agents: Considerations and Caveats. *Nanomedicine* **2008**, *3*, 703−717.
(42) Jonassen, T. E.; Graebe, M.; Promeneur, D.; Nielsen, S.; Christensen, S.; Olsen, N. V. Lipopolysaccharide-Induced Acute Renal Failure in Conscious Rats: Effects of Specific Phosphodiesterase Type 3 and 4 Inhibition. *J. Pharmacol. Exp. Ther.* **2002**, *303*, 364−374.
(43) Moreira, A. L.; Wang, J.; Sarno, E. N.; Kaplan, G. Thalidomide Protects Mice Against LPS-Induced Shock. *Braz. J. Med. Biol. Res.* **1997**, *30*, 1199−1207.
(44) Comper, W. D. Is the LPS-Mediated Proteinuria Mouse Model Relevant to Human Kidney Disease? *Nat. Med.* **2009**, *15*, 133−140.
(45) Zhang, X.; Yin, J.; Peng, C.; Hu, W.; Zhu, Z.; Li, W.; Fan, C.; Huang, Q. Distribution and Biocompatibility Studies of Graphene Oxide in Mice After Intravenous Administration. *Carbon* **2011**, *49*, 986−995.
(46) Klopfleisch, R. Multiparametric and Semiquantitative Scoring Systems For the Evaluation of Mouse Model Histopathology - A Systematic Review. *BMC Vet. Res.* **2013**, *9*, 123.
(47) Shang, S.; Yang, S.-Y.; Liu, Z.-M.; Yang, X. Oxidative Damage in the Kidney and Brain of Mice Induced by Different Nano-materials. *Front. Biol.* **2015**, *10*, 91−96.
(48) Patlolla, A.; Randolph, J.; Kumari, S.; Tchounwou, P. Toxicity Evaluation of Graphene Oxide in Kidneys of Sprague-Dawley Rats. *Int. J. Environ. Res. Public Health* **2016**, *13*, 380.
(49) Sasidharan, A.; Swaroop, S.; Koduri, C. K.; Girish, C. M.; Chandran, P.; Panchakarla, L. S.; Somasundaram, V. H.; Gowd, G. S.; Nair, S.; Koyakutty, M. Comparative *In Vivo* Toxicity, Organ Biodistribution and Immune Response of Pristine, Carboxylated and PEGylated Few-Layer Graphene Sheets in Swiss Albino Mice: A Three Month Study. *Carbon* **2015**, *95*, 511−524.
(50) Liu, J.-H.; Wang, T.; Wang, H.; Gu, Y.; Xu, Y.; Tang, H.; Jia, G.; Liu, Y. Biocompatibility of Graphene Oxide Intravenously Administrated in Mice-Effects of Dose, Size and Exposure Protocols. *Toxicol. Res.* **2015**, *4*, 83−91.
(51) Nurunnabi, M.; Khatun, Z.; Huh, K. M.; Park, S. Y.; Lee, D. Y.; Cho, K. J.; Lee, Y.-k. *In Vivo* Biodistribution and Toxicology of Carboxylated Graphene Quantum Dots. *ACS Nano* **2013**, *7*, 6858−6867.
(52) Chong, Y.; Ma, Y.; Shen, H.; Tu, X.; Zhou, X.; Xu, J.; Dai, J.; Fan, S.; Zhang, Z. The *In Vitro* and *In Vivo* Toxicity of Graphene Quantum Dots. *Biomaterials* **2014**, *35*, 5041−5048.
(53) Zhan, L.; Yanxia, G.; Xiaoyong, Z.; Wei, Q.; Qiaohui, F.; Yan, L.; Zongxian, J.; Jianjun, W.; Yuqin, T.; Xiaojiang, D.; Wangsuo, W. Biodistribution of co-exposure to multi-walled carbon nanotubes and graphene oxide nanoplatelets radiotracers. *J. Nanopart. Res.* **2011**, *13*, 2939−2947.
(54) Randles, M. J.; Woolf, A. S.; Huang, J. L.; Byron, A.; Humphries, J. D.; Price, K. L.; Kolatsi-Joannou, M.; Collinson, S.; Denny, T.; Knight, D.; Mironov, A.; Starborg, T.; Korstanje, R.; Humphries, M. J.; Long, D. A.; Lennon, R. Genetic Background is a Key Determinant of Glomerular Extracellular Matrix Composition and Organization. *J. Am. Soc. Nephrol.* **2015**, *26*, 3021−3034.
(55) Scott, R. P.; Quaggin, S. E. The Cell Biology of Renal Filtration. *J. Cell Biol.* **2015**, *209*, 199−210.
(56) Russier, J.; Treossi, E.; Scarsi, A.; Perrozzi, F.; Dumortier, H.; Ottaviano, L.; Meneghetti, M.; Palermo, V.; Bianco, A. Evidencing a Mask Effect of Graphene Oxide: A Comparative Study on Primary Human and Murine Phagocytic Cells. *Nanoscale* **2013**, *5*, 11234−11247.
(57) Ruggiero, A.; Villa, C. H.; Bander, E.; Rey, D. A.; Bergkvist, M.; Batt, C. A.; Manova-Todorova, K.; Deen, W. M.; Scheinberg, D. A.; McDevitt, M. R. Paradoxical Glomerular Filtration of Carbon Nanotubes. *Proc. Natl. Acad. Sci. U. S. A.* **2010**, *107*, 12369−12374.
(58) Kostarelos, K. Carbon Nanotubes: Fibrillar Pharmacology. *Nat. Mater.* **2010**, *9*, 793−795.
(59) Lacerda, L.; Herrero, M. A.; Venner, K.; Bianco, A.; Prato, M.; Kostarelos, K. Carbon-Nanotube Shape and Individualization Critical for Renal Excretion. *Small* **2008**, *4*, 1130−1132.
(60) Sasidharan, A.; Panchakarla, L. S.; Chandran, P.; Menon, D.; Nair, S.; Rao, C. N. R.; Koyakutty, M. Differential Nano-Bio Interactions and Toxicity Effects of Pristine *Versus* Functionalized Graphene. *Nanoscale* **2011**, *3*, 2461−2464.
(61) De Marzi, L.; Ottaviano, L.; Perrozzi, F.; Nardone, M.; Santucci, S.; De Lapuente, J.; Borras, M.; Treossi, E.; Palermo, V.; Poma, A. Flak Size-dependent Cyto and Genotoxic Evaluation of Graphene Oxide on *In Vitro* A549, CaCo2 and Vero Cell Lines. *J. Biol. Regul. Homeostatic Agents* **2014**, *28*, 281−289.
(62) Guo, M.; Ricardo, S. D.; Deane, J. A.; Shi, M.; Cullen-McEwen, L.; Bertram, J. F. A Stereological Study of the Renal Glomerular Vasculature in the db/db Mouse Model of Diabetic Nephropathy. *J. Anat.* **2005**, *207*, 813−821.
(63) Stolwijk, J. A.; Matrougui, K.; Renken, C. W.; Trebak, M. Impedance Analysis of GPCR-Mediated Changes in Endothelial Barrier Function: Overview and Fundamental Considerations for Stable and Reproducible Measurements. *Pfluegers Arch.* **2015**, *467*, 2193−2218.
(64) Goldwich, A.; Burkard, M.; Ölke, M.; Daniel, C.; Amann, K.; Hugo, C.; Kurts, C.; Steinkasserer, A.; Gessner, A. Podocytes are Nonhematopoietic Professional Antigen-Presenting Cells. *J. Am. Soc. Nephrol.* **2013**, *24*, 906−916.
(65) Brunskill, E. W.; Georgas, K.; Rumballe, B.; Little, M. H.; Potter, S. S. Defining the Molecular Character of the Developing and Adult Kidney Podocyte. *PLoS One* **2011**, *6*, e24640.
(66) Majno, G.; Shea, S. M.; Leventha, M. Endothlial Contraction Induced by Histamine-Type Mediators-Anelectron Microscopy Study. *J. Cell Biol.* **1969**, *42*, 647.

DOI: 10.1021/acsnano.6b03358
ACS Nano 2016, 10, 10753−10767

(67) Babayeva, S.; Zilber, Y.; Torban, E. Planar Cell Polarity Pathway Regulates Actin Rearrangement, Cell Shape, Motility, and Nephrin Distribution in Podocytes. *Am. J. Physiol. Renal Physiol.* **2011**, *300*, F549−F560.
(68) Male, K. B.; Lam, E.; Montes, J.; Luong, J. H. T. Noninvasive Cell-Based Impedance Spectroscopy for Real-Time Probing Inhibitory Effects of Graphene Derivatives. *ACS Appl. Mater. Interfaces* **2012**, *4*, 3643−3649.
(69) Yoon, O. J.; Kim, I.; Sohn, I. Y.; Kieu, T. T.; Lee, N. E. Toxicity of Graphene Nanoflakes Evaluated by Cell-Based Electrochemical Impedance Biosensing. *J. Biomed. Mater. Res., Part A* **2014**, *102*, 2288−2294.
(70) Mu, Q.; Su, G.; Li, L.; Gilbertson, B. O.; Yu, L. H.; Zhang, Q.; Sun, Y.-P.; Yan, B. Size-Dependent Cell Uptake of Protein-Coated Graphene Oxide Nanosheets. *ACS Appl. Mater. Interfaces* **2012**, *4*, 2259−2266.
(71) Yue, H.; Wei, W.; Yue, Z.; Wang, B.; Luo, N.; Gao, Y.; Ma, D.; Ma, G.; Su, Z. The Role of The Lateral Dimension of Graphene Oxide in The Regulation of Cellular Responses. *Biomaterials* **2012**, *33*, 4013−4021.
(72) Li, Y.; Yuan, H.; von dem Bussche, A.; Creighton, M.; Hurt, R. H.; Kane, A. B.; Gao, H. Graphene Microsheets Enter Cells Through Spontaneous Membrane Penetration at Edge Asperities and Corner Sites. *Proc. Natl. Acad. Sci. U. S. A.* **2013**, *110*, 12295−12300.
(73) Tu, Y.; Lv, M.; Xiu, P.; Huynh, T.; Zhang, M.; Castelli, M.; Liu, Z.; Huang, Q.; Fan, C.; Fang, H.; Zhou, R. Destructive Extraction of Phospholipids from Escherichia Coli Membranes by Graphene Nanosheets. *Nat. Nanotechnol.* **2013**, *8*, 594−601.
(74) Adamson, A. W. *Physical Chemistry of Surfaces*; Wiley Interscience: New York, 1990.
(75) Kurien, B. T.; Everds, N. E.; Scofield, R. H. Experimental Animal Urine Collection: A Review. *Lab. Anim.* **2004**, *38*, 333−361.
(76) Park, H. C.; Yasuda, K.; Ratliff, B.; Stoessel, A.; Sharkovska, Y.; Yamamoto, I.; Jasmin, J. F.; Bachmann, S.; Lisanti, M. P.; Chander, P.; Goligorsky, M. S. Postobstructive Regeneration of Kidney is Derailed When Surge in Renal Stem Cells During Course of Unilateral Ureteral Obstruction is Halted. *Am. J. Physiol. Renal Physiol.* **2010**, *298*, F357−F364.
(77) He, C.; Esposito, C.; Phillips, C.; Zalups, R. K.; Henderson, D. A.; Striker, G. E.; Striker, L. J. Dissociation of Glomerular Hypertrophy, Cell Proliferation, and Glomerulosclerosis in Mouse Strains Heterozygous for a Mutation (Os) which Induces a 50% Reduction in Nephron Number. *J. Clin. Invest.* **1996**, *97*, 1242−1249.
(78) Keil, D. E.; Peden-Adams, M. M.; Wallace, S.; Ruiz, P.; Gilkeson, G. S. Assessment of Trichloroethylene (TCE) Exposure in Murine Strains Genetically-Prone and Non-Prone to Develop Autoimmune Disease. *J. Environ. Sci. Health, Part A: Toxic/Hazard. Subst. Environ. Eng.* **2009**, *44*, 443−453.
(79) Chen, S. M.; Mukoyama, T.; Sato, N.; Yamagata, S.; Arai, Y.; Satoh, N.; Ueda, S. Induction of Nephrotoxic Serum Nephritis in Inbred Mice and Suppressive Effect of Colchicine on the Development of this Nephritis. *Pharmacol. Res.* **2002**, *45*, 319−324.
(80) Miyazaki, T.; Ono, M.; Qu, W. M.; Zhang, M. C.; Mori, S.; Nakatsuru, S.; Nakamura, Y.; Sawasaki, T.; Endo, Y.; Nose, M. Implication of Allelic Polymorphism of Osteopontin in the Development of Lupus Nephritis in MRL/lpr Mice. *Eur. J. Immunol.* **2005**, *35*, 1510−1520.
(81) Raij, L.; Azar, S.; Keane, W. Mesangial Immune Injury, Hypertension, and Progressive Glomerular Damage in Dahl Rats. *Kidney Int.* **1984**, *26*, 137−143.
(82) Porter, A. E.; Gass, M.; Muller, K.; Skepper, J. N.; Midgley, P. A.; Welland, M. Direct Imaging of Single-Walled Carbon Nanotubes in Cells. *Nat. Nanotechnol.* **2007**, *2*, 713−717.
(83) Gagliardini, E.; Conti, S.; Benigni, A.; Remuzzi, G.; Remuzzi, A. Imaging of the Porous Ultrastructure of the Glomerular Epithelial Filtration Slit. *J. Am. Soc. Nephrol.* **2010**, *21*, 2081−2089.
(84) Byron, A.; Randles, M. J.; Humphries, J. D.; Mironov, A.; Hamidi, H.; Harris, S.; Mathieson, P. W.; Saleem, M. A.; Satchell, S. C.; Zent, R.; Humphries, M. J.; Lennon, R. Glomerular Cell Cross-Talk Influences Composition and Assembly of Extracellular Matrix. *J. Am. Soc. Nephrol.* **2014**, *25*, 953−966.
(85) Lennon, R.; Singh, A.; Welsh, G. I.; Coward, R. J.; Satchell, S.; Ni, L.; Mathieson, P. W.; Bakker, W. W.; Saleem, M. A. Hemopexin Induces Nephrin-Dependent Reorganization of the Actin Cytoskeleton in Podocytes. *J. Am. Soc. Nephrol.* **2008**, *19*, 2140−2149.
(86) Sumagin, R.; Brown, C. W.; Sarelius, I. H.; King, M. R. Microvascular Endothelial Cells Exhibit Optimal Aspect Ratio for Minimizing Flow Resistance. *Ann. Biomed. Eng.* **2008**, *36*, 580−585.

DOI: 10.1021/acsnano.6b03358
ACS Nano 2016, 10, 10753−10767